CORROSION INHIBITION POTENTIAL OF IMIDAZOLIUM AND PYROLLIDINIUM BASED IONIC LIQUIDS ON MILD STEEL SURFACES IN ACIDIC MEDIUM

A. R. Motsilanyane

orcid.org/0000-0002-2555-1912

B.Sc. (NWU), B.Sc. (Hons) (NWU)

Dissertation submitted in fulfilment of the requirements for the degree *Magister* in Chemistry in the Faculty of Agriculture, Science & Technology at the Mafikeng Campus of the North-West University

Supervisor: Prof Eno E. Ebenso

Graduation October 2017

Student number: 16559363

NORTH-WEST UNIVERSITY
YUNIBESITI YA BOKONE-BOPHIRIMA
NOORDWES-UNIVERSITEIT

DECLARATION

I declare that this project which is submitted in fulfillment of the requirements for the degree of Master of Science (M.Sc.) in Chemistry at North-West University, Mafikeng Campus has not been previously submitted for a degree at this university or any other university. The following research was compiled, collated and written by me under the supervision of Prof. Eno E. Ebenso. All the quotations are indicated by appropriate punctuation marks. Sources of my information are acknowledged in the reference pages.

.....

Andrew Rabontsi Motsilanyane

DEDICATION

This work is dedicated to my Lord and Savior Jesus Christ.

TABLE OF CONTENT

ACKNOWLEDGEMENTS

I would like to take this opportunity to thank my Lord and Saviour Jesus Christ for giving me the grace and willpower to complete this research.

My Supervisor Prof. Eno E. Ebenso, Thank you. It really takes a unique soul like you, with a great vision like the one you have, to transform individuals like me in to being what I am today, through your knowledge and charisma.

Dr. M. M. Kabanda, Dr Y. Sasikumar and Dr. A. S. Adekunle, thank you for your contribution to this project. You were indeed helpful towards this project.

Dr. Lukman and Dr. Fayemi your contribution will never go unnoticed. You are well knowledgeable and I appreciate your selflessness in assisting me. Thank you.

Dr. Chester Murulana and Mr Elija Mashuga, Thank you for every step you took with me, together with Thabo and Masego. It is also through your hard work that I managed to learn from you, through the previous work you carried out.

The following guys Sizwe, Kagiso and Peter, our lab assistants. Guys without you going an extra mile for us, makes it very hard to progress, Therefore, I take this opportunity to thank you as well, for being there when I called for help.

A big thank you to Diseko and Ntsoaki, guys your presence in the lab is greatly felt. It is your motivations and hard work that paved a way to believe in what I was doing. Keep it up.
To the Chemistry Department of North-West University (Mafikeng campus and Potchefstroom), I would like to say Thank you. Not forgetting Mrs Maggy Medupe (late) and Aunty Sophy for all the words of support I received from you.

And to My family, Kitso, Bontsi and Reatlegile, and The Saviour's Embassy Church, I thank you once more, for being there when it mattered most, you're highly favoured.

ABSTRACT

Corrosion inhibition properties of four ionic liquids (ILs) containing both imidazolium and pyrollidium based ILs, namely 1-ethyl-3-methylimidazolium tetrafluoroborate $[EMIM]^+[BF_4]^-$, 1- butyl-2,3-dimethylimidazole tetrafluoroborate $[BDMIM]^+[BF_4]^-$, 1-butyl-1-methylpyrrolidinium bromide $[BMPy]^+[Br]^-$ and 1-ethyl-1-methylpyrrolidinium bromide $[EMPy]^+[Br]^-$ were investigated for mild steel in 1M HCl using electrochemical methods, spectroscopic techniques and quantum chemical calculations. The inhibition efficiency (%IE), increased with increase in concentration of the inhibitor with a maximum value of 90.84% for $[BDMIM]^+[BF_4]^-$, 77.93% for $[EMIM]^+[BF_4]^-$, 80.82% for $[BMPy]^+[Br]^-$ and 87.70% for $[EMPy]^+[Br]^-$ at 500 ppm. The criteria behind the selection of these ionic liquids is based on the fact that they are relatively cheaper and readily available. Presence of imidazole ring in $[BDMIM]^+[BF_4]^-$ and $[EMIM]^+[BF_4]^-$ that contain two nitrogen atoms along with conjugated double bonds resulted into their higher inhibition performance as compared remaining two pyrrolidine based ionic liquids. The difference in their inhibition efficiencies is attributed due to presence of different electron donating alkyl groups. These alkyl groups affect the hydrophobic and solubility of these ionic liquids in addition to the electron density on the donor sites. The tested ionic liquids are structurally related in the sense that both $[BDMIM]^+[BF_4]^-$ and $[EMIM]^+[BF_4]^-$ contain imidazole ring and have different side chains. The higher inhibition efficiency of the $[BDMIM]^+[BF_4]^-$ as compared to $[BMPy]^+[Br]^-$ is attributed to more hydrophobic nature of $[BDMIM]^+[BF_4]^-$ because of electron donating additional methyl and butyl group as compared to $[EMPy]^+[Br]^-$ containing ethyl group as hydrophobic chain. The presence of electron releasing alkyl groups not only enhance the inhibition efficiency due to increase in the hydrophobicity of the inhibitor molecules but also due to increase in the electron density due to their electron donating nature. Similarly, $[BMPy]^+[Br]^-$ and $[EMPy]^+[Br]^-$ are structurally related from each other as both have pyrrolidine ring in their basic structure but different substituents. The higher inhibition performance of $[EMPy]^+[Br]^-$ as compared to $[BMPy]^+[Br]^-$ is attributed to the relatively more solubility and less hydrophobicity of the $[EMPy]^+[Br]^-$ as compared to $[BMPy]^+[Br]^-$. Electrochemical impedance spectroscopy measurements showed that all four inhibitors protect mild steel surface by adsorbing at the steel/hydrochloric acid interface to form protective pseudo-capacitive films. Fourier transform infrared spectroscopy (FTIR) was used to gain more insight into the functional groups involved in the donor acceptor interactions between the inhibitor molecules and mild steel. The changes in the infrared spectra of the ILs before and after mild steel immersion confirm the occurrence of the chemical interactions between the inhibitor molecule and mild steel. Using the UV-Vis, new peaks were observed on $[BDMIM]^+[BF_4]^-$ and $[EMIM]^+[BF_4]^-$ after mild steel immersion, which can be attributed to the transition between π-bonding of Fe/IL complex and the π^* orbital of the anion. The similarity in values of λ_{max} and in the shape for the imidazolium ILs may be due to their

common π-electron nucleus (the imidazolium unit). The broadening of the absorption peak after mild steel immersion is an evidence of the formation of IL/Fe complex. The absorption spectra of the pure ILs show a single absorption peak at 228nm, 223nm, 219nm and 221nm for $[BDMIM]^+[BF_4]^-$, $[EMIM]^+[BF_4]^-$ $[BMPy]^+[Br]^-$, and $[EMPy]^+[Br]^-$ respectively, corresponding to π-π* and/ or n-π* transitions. The Raman bands observed at 758 and 793 cm^{-1} corresponds to C-H vibration. The bands at 1474 and 1540 cm^{-1} correspond to C=C stretching vibrations and the one at 1658 cm^{-1} correspond to asymmetric stretching of $N\text{-}CH_2$ or $CN\text{-}CH_3$ stretching vibration. The main bands at 2918 and 2959 cm^{-1} correspond to asymmetric mode of CH_2 stretching vibration. $BDMIMBF_4$ has intensive bands at 3056 cm^{-1} to 3105 cm^{-1} that correspond to symmetric stretching vibration of CH_3 and CH_2. The characteristic Raman bands observed in pure ILs have disappeared after mild steel immersion. This is an indication of IL/Fe complex formation. Quantum chemical calculations were also used to establish correlations between experimentally determined inhibition efficiencies and molecular quantum chemical descriptors. Both experimental and quantum chemical results showed that the inhibition efficiency of ILs is affected by the length of the alkyl side chain, and the order of inhibition efficiency for the studied compounds is; $[BDMIM]^+[BF_4]^- > [EMPy]^+[Br]^- > [BMPy]^+[Br]^- > [EMIM]^+[BF_4]^-$.

LIST OF ABBREVIATIONS

MS	Mild Steel
ILs	Ionic Liquids
PPM	Parts Per Million
DS	Designer Solvents
GS	Green Solvents
HCl	Hydrochloric Acid
MIC	Microbial Corrosion
IE	Inhibition Efficiency
SCC	Stress Corrosion Cracking
$[HMIM^+][I]^-$	1-Hexyl-3-methylimidazolium Iodide
$[EMIM]^+[BF_4]^-$	1-Ethyl-3 Methylimidazolium Tetrafluoroborate
$[BDMIM]^+[BF_4]^-$,	1-Butyl-2, 3 Methylimidazolium Tetrafluoroborate
$[EMPy]^+[Br]^-$	1-Ethyl-3-Pyrollidinium Bromide
$[BMPy]^+[Br]^-$	1-Butyl-3-Pyrollidinium Bromide
CorriSA	Corrosion Institute of Southern Africa
HIC	Hydrogen-Induced Cracking
VPI	Vapour Phase Inhibitors
VCI	Volatile Corrosion Inhibitors
$4MBPBF_4$	1-Butyl-4-Methylpyridium Tetrafluoroborate
R_P	Polarization Resistance
RTIL	Room Temperature Ionic Liquids

SEM	Scanning Electron Microscopy
EDX	Energy-dispersive X-ray
UV	Ultraviolet Spectrometry
PCE	Platinum Counter Electrode
SCE	Saturated Calomel Electrode
WE	Working Electrode
PDP	Potentiodynamic Polarization
EIS	Electrochemical Impedance Spectroscopy
HOMO	Highest Occupied Molecular Orbital
LUMO	Lowest Unoccupied Molecular Orbital
EA	Electron Affinity
IP	Ionization Potential
ΔE	Energy Gap
DFT	Density Functional Theory
B3LYP	The Becke's Three Parameter Hybrid Functional and the Lee-Yang-Parr Correlation Functional
QSAR	Quantitative Structure Activity Relationship

LIST OF FIGURES

LIST OF TABLES

CHAPTER 1

INTRODUCTION TO CORROSION

1.1 HISTORICAL BACKGROUND

The metallic materials have been widely employed in industries as constructional materials because of their low cost and high mechanical strength. However, these materials are very reactive thereby react with the components of environment and undergo corrosion that affects their performance and lifespan [1]. The selection of these materials is based on their availability, cost effectiveness and mechanical strength. The corrosion affects the several physiochemical properties of the metallic materials like hardness, ductility, density, elasticity, tensile strength and electrical conductivity that limit their use for desired applications. Therefore, corrosion is a worldwide problem to be addressed by developed and developing countries. The most common example of metal corrosion is rust, and that has been around since antiquity. There are many developments which take us back to 1675 by Boyle who discovered the mechanical origin of corrosiveness and corrodibility. This was followed by the discovery of water becoming alkaline during corrosion of iron in 1788 by Austin. Many other developments on the field of corrosion over the centuries occurred including the study of corrosion process with electrochemical impedance spectroscopy by Epelboiu in 1970 [2]. The reduction in strength of structural iron and steel, due to corrosion leads to their serious weakening or failure of such metals. This weakening is caused by their degradation and damage as a result of corrosion [3]. Corrosion can affect the metal in a variety of ways which depend on its nature and the precise environment conditions prevailing and a broad classification of various forms of corrosion. Corrosion can however be controlled but at a substantial cost [4].

1.1.1 DEFINITION OF CORROSION

Corrosion is the gradual destruction of materials (usually metals), by chemical reaction with its environment.

On the other hand the word "rusting" applies to the corrosion of iron and plain carbon steel. Rust is a hydrated iron oxide which appears in the familiar color of red or dark brown. Now ferrous metals such as aluminum, copper and zinc corrode but do not rust [5].

Corrosion destroys metals by converting them into oxides or other corrosion products. Thus corrosion affects the global supply of metals and metallic structures and their replacement consumes a portion of the total supply of the earth`s material resources [2].

1.1.2 CORROSIVE ENVIRONMENTS

Metals can undergo degradation by physical and chemical processes. These various environments includes the soil, the human body, viral marine (Cl, H_2O), Industrial (SO_2, H_2O) the atmospheric indoors (SO_2, H_2O, NH_3 and NO_2), chemicals and viral environments. These environments affects various metal systems such as affect various metal systems such as steels stainless, steels aluminum, aluminum alloys, copper alloys, titanium alloys, nickel alloys metallic and organic coatings depending on the extent of destruction the environment has on the metals [6].

1.1.3 COST OF CORROSION

Corrosion has many consequences and a major one is its effects on the economy of a nation. Various studies have shown that countries like the US incur excessive costs on metallic corrosion of up to 276 billion dollars annually. This represents 3.1% of the US Gross Domestic Product (GDP): Some of the effects of corrosion can be summarized [6] as follows:

- Structural failure or break down (e.g. bridges, cars, aircraft)
- Reduced value of goods due to deterioration of appearance.
- Loss of technically important surface properties of metallic component.
- Production of metal thickness, leading to loss of mechanical strength.
- Mechanical damage to valves, pumps, etc. or blockage of pipes by solid corrosion products [5-7].

1.1.4 TYPES OF CORROSION

Corrosion can affect the metal in a variety of ways which depend on its nature and the environmental conditions. Below are different types of corrosion.

Localized Corrosion: This occurs at specific locations, local anodes and cathodes on the metallic surface. The three most prevalent forms of localized corrosion are (i) pitting (ii) crevice corrosion (iii) stress-corrosion cracking.[8]

Pitting corrosion: pitting is a form of localized corrosion in which the attack is confined to a small fixed area of the metal surface. It occurs due to localized breakdown of a passive film,

usually by chloride ions. It is a dangerous form of corrosion attack for several reasons. Pits can results in the perforation of a metal component while the rest of the metal piece remains unattached. In the presence of applied stress, pits can serve as sites to initiate stress-corrosion cracking, another catastrophic form of corrosion attack [8]. Pits can require a long time to appear in actual service (months to years) so that their absence in the short term is not a certainty that the metal or alloy is immune to pitting corrosion, although most experimental studies have involved stainless steels and their alloying component, aluminum and copper [9]. Pitting is caused by the presence of an "aggressive" anion in the electrolyte, usually Cl^- ions, but pitting of various metals or alloys has also occurred in the presence of other anions, including I^-,$S_2O_4^-$, or NO^- [10,11].

Crevice corrosion: Crevice corrosion is a form of localized corrosion that occurs within narrow clearance or under shielded metal surface. It occurs in geometrical clearance such as under quartets or seals, under bolt heads, within screws threads [12].

Stress corrosion cracking: Stress corrosion cracking is the cracking of a metal or alloy by the combined action of stress and the environment. Stress corrosion cracking (SCC) can occur in stressed structured such as bridges and support cables, aircraft, pressure vessels, pipelines, and turbine blades. During the stress corrosion cracking most of the metal or alloy is virtually unattached [13].

Corrosion Fatigue: Corrosion fatigue is the cracking of a metal or alloy due to the combined action of a repeated cyclic stress and a corrosion environment. It can occur in aircraft wings, in budges and vibrating luminary [12, 13].

Cavitation corrosion: Cavitation corrosion is the combined mechanical and corrosion attack caused by the collapse and impingement of vapor bubble in a liquid near a metal surface. It can occur in ship propels, within pumps, on turbine blades, on hydrofoils and on surface where there is a high velocity fluid flow and where pressure changes are uncounted [14]. Cavitation corrosion occurs when the flow of a corrosion liquid products are localized low pressure which leads to the formation of bubbles in the liquid. These low pressures necessary to form bubbles can be caused by the fluid flow across curved interfaces. The force of the collapse of their bubbles involves creation of shock waves and high-velocity Mino sects [15].

Erosion Corrosion: In erosion corrosion the mechanically effect is provided by the movement of a corrosion liquid against the metal surface, without the need for a metal caused

by the movement of a corrosion liquid against the metal surface. The velocity of the fluid play an important role in erosion corrosion and increase in velocity generally lead to increase in erosion corrosion [16]. Turbulent flow results in an increased contact to the fluid with metal surface compared to laminar flow and caused more damage than laminar flow [17].

Fretting Corrosion: In the Fretting corrosion the protective measures include the use of additional of corrosion inhibitors [16, 17]. It occurs at the contact area between two materials under load and subject to minute relative motion by vibration or some other force. Fretting corrosion is cured by the slight periodic motion of the surface rubbing against each other and is due to the combined effects of wear and corrosion. Fretting corrosion can be reduced by various measures [17, 18]. These include the use of lubricants which includes friction and acts as corrosion inhibitors.

Galvanic Corrosion: Galvanic corrosion occurs when two dissimilar metals are in physical (and electric) contact in aqueous electrolyte. [19] Examples of galvanic corrosion include the following:

- Zinc – coated screws in a sheet of copper
- Copper piping that is connected to steel tanks

Waterline Corrosion: A corrosion of partially immured metals at a location just below the waterline, the level of submissions (figure 1.1). The electrolyte areas near whereas electrocute areas below the oxygen Concentration cell is established with the upper concentration cell is established with the upper part of the metal acting as an anode [20].

Uniform Corrosion: The metal is attacked more or less evenly over its entire surface (figure 1.2). No portions of the metals surface are attacked more preferentially than others, and the metal piece is thinned away by the process of corrosion until the piece of zinc in hydrochloric acid [21].

Intergranular Corrosion: Is the pronounced localized attack that occurs in narrow regions at or immediately adjacent to grain boundaries on the alloy (figure 1.3). The stainless steel is said to be sensitized and is susceptible to intergranular corrosion. During scutization, carbon diffuses to the grain boundaries where it combines with chromium to form chromium carbide precipitate (such as Cr_{23} C_6) [23]. This process deplets chromium from the areas in and adjacent to the grain boundaries so that the regions locally contain less than the 12% Cr required for a stainless steel. Thus, localized corrosion occurs in certain areas in the form of intergranular corrosion [22].

Figure 1.1: Waterline corrosion

Figure 1.2: Uniform corrosion

Figure 1.3: Intergranular corrosion

Figure 1.4: Filiform Corrosion

Filiform Corrosion: The mechanism for corrosion allows water and oxygen migrate. The dissolved oxygen has its highest concentration at the back of the head. When the oxygen is reduced in the tail region, the metal ion dissolution and formation proceeds to the head (figure 1.4). This type of corrosion has a tendency of taking place in conditions with a high level of humidity. Nitrates, sulfates and carbonates and condensates that contain halides have been associated with filiform [22].

1.1.5 RATE OF CORROSION

Corrosion rate refers to how fast a metal is being consumed by corrosion process. These include weight loss per unit area per time penetration rates and electrochemical rates. Corrosion rates can be expressed as various units used in expressing corrosion rate include Weight loss, g/cm ^{2} h, g/cm^2 day, g/m ^{2} h, mg/m^2 s, mdd (mg/dm^{2}day) ; Penetration, ipy (includes per year), mpy (mils per year), mmy (millimeter per year), mm (milli meter per year) ; Corrosion Current Diversity,m A/cm^2,m A/cm^2, A/cm^2, A/m^2. Weighed metal sample are removed from the solution or the environment at various time intervals and the loss in weight due to metallic corrosion is determined, per unit area of the sample. Tight and adherent corrosion products can be removed by chemical or electrochemical methods/ which are usually specific to the metal or the alloy being tested. The corrosion rate is simply the slope of the straight line. The instantaneous corrosion rate at any given time is the slope of the tangent line drawn at that given time [24].

1.1.6 FACTORS THAT AFFECT THE RATE OF CORROSION

There are several factors that affect the rate of corrosion and can be divided into two parts, which are factors affecting the metal and factors affecting corrosive environment. The factors affecting metal include; [25]

A. Nature of the metal: The tendency of the metal to undergo corrosion is mainly dependent on the nature of the metal. Generally the metals with lower electrode potential have more reactive and more susceptible for corrosion, example, metals like K, Na, Mg, Zn have low electrode potential and undergo corrosion very easily, in comparison with noble metals like Ag, Au, Pt which have higher electrode potential and thus have negligible corrosion rate.

B. Surface state of the metal: The corrosion product is usually the oxide of the metal; the nature of the product determines the rate further corrosion process. Metals like Al, Cr, Ti have an oxide layer on the surface which is stoichiometric, highly insoluble and non-porous in nature with low ionic and electronic conductivity, thus that type of products layer effectively prevents further corrosion. The opposite goes for metals such as Zn, Fe, Mg which the oxide layer formed on the metal surface is non-stoichiometric, soluble, unstable and porous in nature, thus they cannot control corrosion on the metal surface.

C. Anodic and Cathodic area: Rate of corrosion is greatly influenced by the relative sizes of cathodic and anodic areas. If the metal has smaller anodic area and larger cathodic area

exposed to corrosive atmosphere, more intense and faster is the corrosion occurring at anodic area because at anode oxidation takes place and electrons are liberated. At the cathode these electrons are consumed. If the cathode is smaller than the reverse process takes place, a decrease of the rate of corrosion.

D. Hydrogen over voltage: A metal with low hydrogen over voltage on its surface is more susceptible for corrosion. When the cathodic reaction is hydrogen evolution type with low hydrogen over voltage, liberation of H_2 gas is easier so that cathodic reaction is very fast, that makes anodic reaction faster hence overall corrosion process is very fast. If the H_2 over voltage is high so cathodic reaction is slow hence corrosion reaction.

Now factors that affect the rate of corrosion.

For corrosion to occur, four main elements must be present, and these collectively are referred to as the corrosion cell: an anode (+), a cathode (-), a metallic conductor and an electrolyte. Five factors that do play a highly important role in determining corrosion rates are as follows; [25]

Oxygen: Like water, oxygen increases the rate of corrosion; yes corrosion can take place in an oxygen deficient environment but not as rapid and quick as in an oxygen sufficient environment.

Temperature: It has been proven beyond doubt that the higher the temperature the faster the corrosion, thus corrosion occurs rapidly in warmer environments than in cooler ones

Chemical Salts: Chemical salts increase the rate of corrosion by increasing the efficiency (conductivity) of the electrolyte. The most common chemical salt is sodium chloride, a major element of seawater, one must note that sodium chloride is a hygroscopic materiel, that is, it

extracts moisture from the air which then increases the rate of corrosion in non-immersed areas.

Humidity: Humidity and time of wetness play a large role in promoting and accelerating the rate of corrosion. Time of wetness refers to the length of time an atmospherically exposed substrate has sufficient moisture to support the corrosion process, thus the wetter the environment, the more corrosion is likely to occur.

1.1.7 KINETICS AND THERMODYNAMICS OF CORROSION

1.1.7.1 Effect of Temperature

The corrosion rate increases with increasing temperature. An effect of temperature on the corrosion rate of iron in water open to the atmosphere and containing dissolved Oxygen, shows that corrosion rate first increases with increasing temperature up to 80^0C and then decreases with further increase in temperature [26]. Two competing effect at work. First the diffusion coefficient increases with temperature. The second temperature effect is that the concentration of dissolved O_2 decreases with the increasing temperature [25].

1.1.7.2 Effect of Sound Velocity

Increasing the velocity of the sol brings executants up to the electrode surface more easily, thus reducing the thickness of the oxygen diffusion layer. As decreases the value of the value of the limiting diffusion content will increase [25, 26].

1.1.7.3 Effect of Oxygen Concentration

Increasing the concentration of dissolved O_2 increases the limiting current deity. Various experimental studies have shown that the corrosion increases with increasing O_2 content of the electrolyte. Uhlig et al have observed that for the corrosion of wild steel in water containing small amounts of $CaCl_2$, the corrosion rate increases with increasing O_2 concentration [27]. In systems where the corrosion rate is uneven the control of the oxygen reduction reaction, the addition of certain chemical compounds can reduce the corrosion rate by reducing the concentration of dissolved O_2. These chemicals are called "Oxygen Scavengers" and two that are used frequently are Sodium Sulfite (Na_2SO_3) and Hydrazine (N_2H_4) [28].

1.1.7.4 Area Effects in Galvanic Corrosion

Increasing the cathode area results in an increase in the value of the limiting diffusion current when copper and iron are coupled in sea water iron is the diode and copper is the cathode. The corrosion rate increases with the area of the cathode [29]. The open-circuit corrosion potential for uncoupled zinc is more negative than for iron, so when the two metals are coupled the zinc electrode is the diode of the pair. The corrosion rate of zinc in the Fe/Zn couple is higher than the corrosion rate of uncoupled zinc [30-32].

1.1.7.5 Hydrogen Ion Concentration of the Solution

Hydrogen reduction reaction in industrial air-free, H_2 saturated solutions can undergo concentration polarization, in which it is seen that the limiting diffusion current density for hydrogen reduction increases with decreasing pH (i.e. with increasing acidity) [33].

1.1.8 MECHANISM OF CORROSION

Corrosion can either be cathodic or anionic, so the work of the inhibitor is to bind either at the cathodic part or the anionic part to reduce, if not to prevent the electrons or protons from the metal from reacting with the environment like water. Corrosion is an electrochemical process, i.e. corrosion usually occurs not by direct chemical reaction of a metal with its environment but rather through the operation of coupled electrochemical half-cell reaction. A half cell reaction is one in which electrons appear on one side or another of the reaction as written. If electrons are products (right hand side of the reaction), then the half-cell reaction is a reduction reaction [33, 34]. The loss of metal occurs as an anodic reaction. This is an anodic reaction because a given species undergoes oxidation, i.e. there is an increase in its oxidation number and there is a loss of electrons at the anodic site (electrons are produced by the reaction). Cathodic reaction, a given species undergoes reduction i.e. there is a decrease in its oxidation number and there is a gain of electrons at the cathodic site (electrons are consumed by the reaction. On a corroding surface diode and cathodic reactions occurs in a coupled number at different places on the metal surface. At certain sites on the iron surface, iron atoms pars into solution as Fe^{2+} ions by e.g. The two electrons produced by these anodic half-cell reactions are consumed elsewhere on the surface to reduce two hydrogen ions to one H_2 molecule [32-34]. The reason that two different electrochemical half-cell reactions can occur on the same metal surface lies in the heterogeneous nature of a metal surface. Therefore corrosion is the simultaneous transfer of mass and change across a metal solution interface [34].

Metal atoms at the highest energy sites are most likely to pass into solution. These high energy sites include atoms at the edges and corners of crystal planes, for example stressed surfaces also contain atoms that are reactive because they have a less stable crystalline environment. There are four conditions which are necessary for corrosion which are necessary for corrosion to occur. These are the following: an anodic reaction, cathodic

reaction, and a metallic path of contact between anodic and cathodic sites, the pressure of an electrolyte [35]. An electrolyte is a solution which contains dissolved ions capable of conducting a current. The most common electrolyte is aqueous solution i.e. water containing dissolved ions. The need for the pressure of an electrolyte as a condition for corrosion to occur is illustrated by the phenomenon of atmosphere corrosion i.e. the corrosion of metals in the mutual outdoor atmosphere [30]. Vennon observed that a critical relative humidity exist below which atmospheric corrosion is negligible and above which corrosion is negligible and above which corrosion occurs. It can be seen that the corrosion of iron occurs above 69% relative humidity [35].

The critical relative humidity is the condition where multimolecular buyers of water vapor physical absorb from the atmosphere onto the oxide covered metal surface [36]. Cathodic reaction are thus very Important, first as seen above the cathodic reaction is coupled to the cathodic reaction so that impending the cathodic reaction will also impend the anodic reaction. Similarly, accelerating the cathodic reaction will also accelerate the anodic reaction. In addition, cathodic reaction may induce corrosion through secondary effects by the products of the catholic reaction. In stress corrosion cracking crack limit the exchange of dissolved metal ions with the bulk electrolytes, thus metal cations in this can be Fe^{+} ion, accumulate within the stress corrosion crack and then hydrolyzed to form hydrogen ions [34-36]. The local environment within the crack tip becomes acidified due to the production of hydrogen ion. In acidic solutions, the major cathodic reaction is the reduction of hydrogen cons. Thus hydrogen ions produced within the crack can be reduced to form hydrogen atoms which absorb on the metal surface. Some of these hydrogen atoms then migrates into the stressed region ahead of the crack tip. The pressure of hydrogen atoms in stressed areas prompts the growth of hydrogen embrittlement [32, 35].

Mechanism of corrosion can follow one the following processes; the inhibitor is chemically adsorbed (chemisorption) on the surface of the metal and forms a protective thin film with inhibitor effect or by combination between inhibitor ions and metallic surface or the inhibitor leads a formation of a film by oxide protection of the base metal or the inhibitor reacts with a potential corrosive component present in aqueous media and the product is a complex. A piece of bare iron left outside where it is exposed to moisture (in salt and water), the

corrosion rate is enhanced by an electrochemical process in which a water droplet becomes a Voltaic cell, in contact with the metal, oxidizing the iron [37].

The oxidizing iron supplies electrons at the edge of the droplet to reduce oxygen from the air. The iron surface inside the droplet acts as the anode for the process

$$Fe\,(s) \rightarrow Fe^{2+}(aq) + 2e^{-} \qquad (1)$$

The electrons can move through the metallic iron to the outside of the droplet where

$$O_2\,(g) + 2H_2O\,(l) + 4e \rightarrow 4\,OH^{-}\,(g) \qquad (2)$$

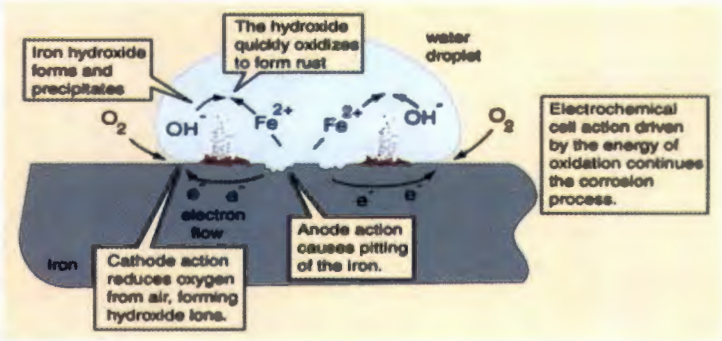

Figure 1.5: Mechanism of Corrosion

Within the droplet, the hydroxide ions can move inward to react with iron (II) ions moving from the oxidation region.

Iron (III) hydroxide is precipitated

$$Fe^{2+}(aq) + 2OH^{-}\,(aq) \rightarrow Fe(OH)_2\,(s) \qquad (3)$$

Rust is then quickly produced by the oxidation at the precipitate

$$2Fe(OH)_2(s) + O_2(g) \rightarrow 2Fe_2O_3 + H_2O\,(l) \qquad (4)$$

The rusting of the unprotected iron in the presence of air and water is the inevitable because it is driven by an electrochemical process. However other electrochemical processes can offer some protection against corrosion, e.g. Cathodic protection and anodic protection [37, 38].

Underground steel pipes offer the strength to transport fluids at high pressures, but they are vulnerable to corrosion driven by electrochemical processes. A measure of protection can be offered by driving a magnesium rod into the ground near the pipe and providing an electrical connection to the pipe. Since the magnesium has a standard potential of -2.83 volts compared

to -0.41 volts for iron, it can act as anode of a voltaic cell with the steel pipe acting as the cathode [38].

1.1.9 CLASSIFICATION OF CORROSION

Depending upon the nature of corrosion, and the factors affecting it, corrosion may be classified into the following processes: [39]

- Chemical corrosion
- Bio- chemical corrosion
- Electrochemical corrosion

Chemical corrosion

This is the wearing away due to chemical reactions, mainly oxidation-reduction reactions. It occurs whenever a gas or liquid chemically attacks an exposed surface, often a metal. This process is accelerated by warm temperatures including acids and salts. The processes of reduction-oxidation reactions require species of a material that is oxidized (the metal) and another that is reduced (the oxidizing agent). The complete reaction can be divided into two partial reactions, that is, oxidation and the other reduction. In oxidation, the metal loses electrons, and this section is known as the anode. In the reduction reaction, the oxidizing agent gains the electrons that have been shed by the metal, and the zone in which this happens is the cathode [40].

Bio- chemical corrosion

Microbiological corrosion is the deterioration of materials caused directly or indirectly by bacteria, fungi, moulds, algae or a combination of microbial species. Bacterial corrosion is possible under aerobic conditions. In this situation corrosion is often the result of the production of corrosive metabolite; or, may be caused by bacteria like *Ferrobacillus Ferrooxidants* that may directly oxidize iron into iron oxides or hydroxides. This may sometimes lead to the formation of deposits with the creation of oxygen concentration cells [39,40].

Electrochemical corrosion

This is defined as the corrosion of a metal associated with the flow of electric current in electrochemical corrosion of iron. Corrosion often begins at a point where the metal is under stress and that can be a bent location on the metal. Sometimes it takes place at the a location where two pieces of metal are joined together, or under a loosely-adhering paint film. The

metal ions then dissolves in the moisture film and this environment causes the electrons to migrate to another location. These electrons are later taken by depolarizer. Oxygen is the most common depolarizer; the resulting hydroxide ions react with the Fe^{2+} to form the mixture of hydrous iron oxides known as rust [39-41].

From the beginning parts of the metal that can serve as an anode and cathode can depend on many factors, as can be observed from the irregular corrosion patterns that are commonly observed. An anodic region is sometimes detected on forming or machining on regions that have undergone stress. This region tends to have higher free energies [42].

1.2. CORROSION INHIBITION

1.2.1 DEFINITION OF CORROSION INHIBITION

A corrosion inhibitor is any chemical substance which when added to a solution increases the corrosion resistance. Corrosion inhibitors can be incorporated into paints or organic coatings corrosion inhibitors modify electrochemical reactions by their actions from the solution metal/ solution interface and the increase in corrosion resistance can be measured by various parameters [34].

1.2.2 TYPES OF INHIBITORS

Inhibitors can be classified in to anodic, cathodic, mixed and Volatile corrosion inhibitors.

Anodic inhibitors

Anodic Inhibitors are chemical substances that form a protective layer of oxide film on the surface of the metal, causing resistance to corrosion. This protective layer causes a large anodic shift. This shift forces a metallic surface into passive passivation region and they are also called passivators. Anodic corrosion inhibitor mechanisms involve blocking of anodic sites in an electrochemical cell. The blocking of the anodic sites depends on concentration of the inhibitor [40].

Cathodic inhibitors

Cathodic inhibitors slow the reaction at the cathode or precipitate cathodic areas in order to increase the impedance on the surface, limiting diffusion of reducible species. Some cathodic inhibitors work by making the recombination and discharge of hydrogen more difficult. But other cathodic inhibitors such as calcium, zinc or magnesium, may be precipitated as oxides to form a protective layer on the metal [41, 42].

Mixed inhibitors

Mixed inhibitors work by reducing both the cathodic and anodic reactions. They form film of compounds that results to the formation of precipitates on the surface, blocking both anodic and cathodic sites. When hard water is used that is high in calcium and magnesium, this becomes less corrosive than soft water because of the tendency of the salts in the hard water to precipitate on the surface of the metal forming a protective film. Silicates and the Phosphates are the most common inhibitor in the category of formation of precipitates. Sodium silicate, for example, is used in many domestic water softeners to prevent the occurrence of rust water [43].

Volatile corrosion inhibitors

Volatile corrosion inhibitors are also known as vapor corrosion inhibitors. They are chemical substance that is added to the surface of a paper. Whenever there is a metal that needs to be protected it is covered with this paper, and these chemicals are slowly volatilized and release compounds within a sealed airspace that actively prevents surface corrosion of the metal. Covering metals in volatile corrosion-inhibitor-coated paper provides a short-term protection against corrosion. The chemicals in the paper continuously vaporize to insulate sensitive parts against moisture and humidity [44].

1.2.3 CORROSION IN DIFFERENT MEDIA

Corrosion can take place in different kinds of media. These include atmosphere environment, oil and water. The most common media in which corrosion takes place include metal or basic solutions and acidic or alkaline solutions. In metal or basic solutions the major cathodic reaction is the reduction of dissolved oxygen,

$$O_2\,(g) + 2H_2O + 4e \rightarrow 4OH\,(aq) \qquad (5)$$

The hydrogen ions are produced by this cathodic reaction. In a thin layer electrolyte, such as that which exists in atmospheric corrosion, the continued production of OH ions and their accumulation will cause an increase in the pH of the thin layer of solution. If the PH increases the solution become more alkaline. Aluminium for example has a low corrosion rate at pH7 but the corrosion rate increases dramatically with increasing pH [35, 36].

1.2.4 TECHNIQUES OF APPLICATION OF CORROSION INHIBITORS

The most usefully technique to analysis the effectiveness of an inhibitor are weight loss experiment and electrochemical measurements, like polarization curve method and the

impedance measurement analyzing. In addition, microscopy techniques are used to characterize the corrosion process [30, 31].

1.2.5 EFFECTS OF CORROSION

Natural corrosion causes the collapse of buildings, airplane crashes, refinery and factory explosions, directly costing the economy about R130-billion a year to the research and development organization [45]. In 2005 University of the Witwatersrand study puts the estimated direct cost of corrosion at R154-billion per year. This figure is higher than that estimated by Mintek. Other International support from an Electric Power Research Institute of the US study, which shows that more than half of all unplanned power outages are due to corrosion. Also a study showed that different countries indicate that between 25% and 30% of water supply is lost in the supply chain due to corrosion [45,46].

However corrosion can be prevented by applying known corrosion technology. The effects of corrosion includes economical loss, waste of energy and materials, environmental impact and safety, and this is a national crisis. The estimated cost of corrosion worldwide is said to be greater than US$1.8-trillion, while in South Africa, the direct cost of corrosion is estimated to be around R130-billion [46]. Half of every ton of steel that is produced, is produced merely to replace corroded steel. This implies a significant carbon footprint, as 380 kg of carbon dioxide (CO_2) is produced for every ton of steel produced. However, several independent studies have also shown that 25% of the abovementioned effects and costs of corrosion can be prevented by applying known technology. This places a significant emphasis on the importance on corrosion education [45]. Institutions like Mintek in South Africa helps industries to reduce the adverse impacts of corrosion by performing failure investigations, aiding in material selection, and providing advice. Mintek also performs failure investigations in order to identify what causes the problem of metal corrosion. This helps to prevent costly failures for future structures [46].

1.2.6 CORROSION OF MILD STEEL

One of the major materials in constructional material is mild steel. It is widely used to due to its excellent mechanical properties and low cost. Hydrochloric acid solutions are widely used in several industrial processes, like acid pickling of steel, chemical cleaning and processing,

and ore production, because of the general aggression of acid solutions. Therefore, inhibitors are commonly used to reduce and to impede the attack on the metal surface. The following factors plays an important role in selection of inhibitor and that is; the selection of an inhibitor is controlled by its economic availability, its efficiency to inhibit the substrate material, its environmental side effects and its ability to maintain the surface of the material. Studies have revealed that excellent acid inhibitors for corrosion of steel in acidic medium are organic compound containing nitrogen, oxygen and/or sulphur atoms [47,48]. The inhibiting action of these compounds is attributed as a first stage, to the adsorption of the additives to the metal/solution interface. The adsorption process depends upon the nature and surface charge of the metal, the type of aggressive media, the structure of the inhibitor and the nature of its interaction with the metal surface. Some cationic surfactants such as, mono and diatonic benzothiazolic quaternary ammonium bromide, alkyl dimethyl isopropyl ammonium hydroxide, new schiff base cationic surfactants, are used as inhibitors for corrosion of steel in acidic solutions. They inhibit the corrosion by the adsorption on the steel surface Cationic surfactants can be easily synthesized from relatively cheap raw materials, nontoxic and have surface active property [47].

1.2.7 CORROSION CONTROL MEASURES

Corrosion control refers to measures that are implemented in various fields to control corrosion in soil, metal, concrete, water and sand. This consists of different corrosion monitoring and control techniques that can be utilized by industries to solve corrosion problems according to their requirements. With such measures, the harmful effects and negative consequences of corrosion can be avoided [48]. Corrosion can lead to countless environmental issues. For example, ships, tankers and pipelines are often subjected to the dangerous corrosion effects. Corroded water systems can also contaminate drinking water. These serve as threats to the environment and mankind, so effective corrosion control methods should be implemented to prevent the damaging effects of corrosion. Corrosion can be controlled in several ways: [30, 45, 46] namely;

Cathodic protection

This technology utilizes direct current to counteract a metal structure's corrosion, in structures like gas pipelines and storage tanks. This helps prevent the onset of corrosion and even stop it from worsening [46].

Linings and coatings

These serve as the main tools for fighting corrosion. They are usually applied in combination with CP to achieve the highest level and most cost-effective corrosion protection [45, 46].

Corrosion inhibitors

These are substances that, when placed in a certain environment, reduce the corrosion rate of that environment to certain materials like metal. These can be beneficial in extending the lifespan of equipment and preventing failures as well as system shutdowns. Corrosion inhibitors can also prevent heat transfer loss, contamination and preserve the aesthetic appearance of the structures. Selection of materials refers to choosing materials that are corrosion resistant like special alloys, plastic and stainless steel to improve the lifespan of structures [47].

1.2.8 AIM AND OBJECTIVES OF THE PRESENT STUDY

The aim of this study is to investigate the inhibitive effects of two imidazolium and two pyrollidinium based ionic liquids on mild steel corrosion in 1M HCl.

Specific objectives are to:

- Apply thermodynamics, kinetics and adsorption principles in studying the inhibition potential of ionic liquids, that is, the effect of ionic concentration and temperature on the corrosion rate.
- Investigate the effect of cationic head groups on corrosion inhibition potential of imidazolium and pyrollidinium ionic liquids.
- Propose the possible inhibition mechanism, type of adsorption and adsorption isotherm for corrosion inhibition.
- Use Fourier transform infrared spectrometry (FTIR), Raman and ultraviolet spectrometry (UV) to study the interface interactions between the ionic liquids and the metal surfaces to determine the mode of interfacial reactions and to investigate the interaction between ionic liquids and metals to see the functional groups that have interacted.
- Use some quantum chemical/theoretical techniques e.g. density functional theory (DFT) and to calculate quantum chemical parameters of the inhibitors and correlate them with the experimentally obtained inhibition efficiency.

CHAPTER 2

LITERATURE REVIEW ON IONIC LIQUIDS

2.1 IONIC LIQUIDS

2.1.1 HISTORICAL BACKGROUND OF IONIC LIQUIDS

The first conference on ionic liquids took place in Salzburg in 2005. The two points of significance in modern ionic liquids is their low vapour pressures, in most instances which contrast the environmental problems of volatile organic solvents and moderate specific conductivities, usually in the same range as those of aqueous electrolytes. It is found that many such systems are excellent solvents or catalysts for organic reactions [51]. Ionic liquids therefore dissociate to some extent at least into ions, having a conductivity which can be captured. One other important aspect about ionic liquids is their molarity regarding kinetic measurements, including conductivity. Molarity is the amount of substance concentration. The modern ionic liquid must consist of ions and ion pairs, (undissociated molecules), while liquid alkali halides are purely ionic and aqueous electrolytes' behave as a mixture of hydrated ions and the molecular solvent water [41].

Ionic liquids can be compared to proton chemistry in water in the following ways: firstly acidic protons in ionic liquids often occur as anions e.g. HBr_2^-, HCl_2^-, rather than cations. Secondly, protons bonded to bases such as pyridine and 1-methylimidazole are not labile. Bases in ionic liquids appear to act in accordance with their gas phase proton affinities (1-methylimidazole>pyridine>ammonia). These bases do not behave in line with their pK_b's in water.

When water is added to an ionic liquid the following process may occur [42]:

1) Some anions such as $AlCl_4^-$ and HCl_2^- are irreversibly decomposed.
2) Water may bind strongly to one of the ions.
3) Water may dissolve the liquid until it forms a saturated salt solution.
4) At high temperature, species such as $Li(H_2O)^+Cl^-$ may decompose to LiOH and HCl

Once we have established from conductivity measurements that, a liquid is ionic, its temperature and complexity should not pose special problems for using it as a solvent for electrochemical analysis. Ionic liquids can be detected by very low vapour pressures, with their NMR data showing BR^+A^- and BR^+A^- forming dissociation. The breakdown of BR^+A^- (e.g. EMIMCl) into B and RA is irreversible whereas, for the acid-base system the vapor may consist of the ionic compound and the behavior of the vapour should correlate with the gas phase proton affinities [43-45, 52a]. Literature, survey reveals that previously several corrosion inhibitors have been used for the inhibition of metallic corrosion in various

aggressive media [52b-c]. Ezhilarasi *et al.* [52b] described the inhibition characteristics of (1-acetyl-4, 5-dihydro-5-phenyl-3-(thiophen-2yl) pyrazoles ionic liquid on mild steel corrosion in acidic solution using weight loss, electrochemical impedance spectroscopy and potentiodynamic polarization methods. Results showed that investigated ionic liquid acts as mixed type inhibitor and its adsorption obeyed the Langmuir adsorption isotherm. Weight loss results showed that tested ionic liquid showed highest inhibition efficiencies of 66.67% and 85.71% in HCl and H_2SO_4 media, respectively at 0.4% concentration. Similar observation was reported by Manamela et al. [52c] while studying the inhibition effect of 1-butyl-3-methylimidazolium tetrafluoroborate [BMIM][BF4-] and 1-decyl-3-methylimidazolium tetrafluoroborate [DMIM][BF4-] on zinc corrosion in acidic solution. Both the tested ionic liquids show very low inhibition efficiency of in the testing medium at 500 ppm concentration. In view of the lower inhibition efficiencies of these and several other ionic liquids those showed relatively lower inhibition efficiency, the development of the new ionic liquids of high inhibition performance is highly anticipated. The ionic liquids tested in the present works showed good inhibition efficiency towards mild steel corrosion in acidic solution. Results showed the $[BDMIM]^+[BF_4]^-$, $[EMIM]^+[BF_4]^-$, $[BMPy]^+[Br]^-$ and $[EMPy]^+[Br]^-$ gave the inhibition performance of 90.84%, 77.93%, 80.82% and 87.70%respectively, at 500 ppm concentration.

2.1.2 DEFINITION OF IONIC LIQUIDS

An ionic liquid is a salt in which the ions are poorly coordinated, which result in the solvent being liquid below the formation of a stable crystal lattice. The methylimidazolium and pyridinium ions have proven to be good starting points for the development of ionic liquids. The term "designer solvent" is also given to ionic liquids meaning that the properties such as melting points, viscosity and solubility of a starting material and other solvent are determined, that is, their synthesis allows a chemist to know exactly what their function is going to be at the end [52].

2.1.3 SYNTHESIS OF IONIC LIQUIDS

Most ionic liquids are formed from cations that do not contain acidic protons. The most common classes of cations has low melting point, such as complex polycationic amines and heterocycle-containing drugs, have also been prepared. The synthesis of ionic liquids can generally be split into two sections: the formation of the desired cation and anion exchange

where necessary to form the desired product [50]. In some cases only the first step is required, as with the formation of ethylammonium nitrate. In many cases the desired cation is commercially available at reasonable cost, most commonly as a halide salt, thus requiring only the anion exchange reaction. Examples of these are the symmetrical tetraalkylammonium salts and trialkylsulfonium iodide. The discovery that the imidazolium-based salts also generally displayed lower melting points than the 1-alkylpyridinium salts used prior to this cemented their position as the cations of choice since then. Indeed, the method reported by H. Huang, for the preparation of the [RMIM]Cl/$AlCl_3$-based salts remains very much that employed by most workers to this day [50-52].

2.1.4 PROPERTIES OF IONIC LIQUIDS

Ionic liquids have relatively low melting points. The distinction is based on the salt exhibiting liquidity at or below a given temperature, often taken to be 100 °C. Ionic liquids contain organic cations rather than inorganic ones. Room-temperature ionic liquids containing organic cations including quaternary ammonium, phosphonium, pyridinium, and – in particular – imidazolium salts are currently available in combination with a variety of anions and have been studied for applications in electrochemistry and in synthesis. It should be emphasized that ionic liquids are simply organic salts that happen to have the characteristic low melting point. Many ionic liquids have been widely investigated with regard to applications other than as liquid materials: e.g. as electrolytes, phase-transfer reagents, surfactants and fungicides and biocides: wide liquid ranges exhibited by ionic liquids, combined with their low melting points and potential for tailoring size, shape, and functionality, offer opportunities for control over reactivity unobtainable with molecular solvents. It is worth noting that quaternary ammonium, phosphonium, and related salts are being widely reinvestigated as the best ionic liquid choices for particular applications, particularly in synthetic chemistry, are reevaluated. Changes in ion types, substitution, and composition produce new ionic liquid systems, each with a unique set of properties that can be explored and hopefully applied to the issues. The simplest ionic liquids consist of a single cation and single anion. More complex examples can also be considered, by combining of greater number [51, 52, 53]. Chloroaluminate (III) ionic liquid systems are perhaps the best established and have been most extensively studied in the development of low-melting

organic ionic liquids with particular emphasis on electrochemical and electrode position applications, transition metal coordination chemistry, and in applications as liquid Lewis acid catalysts in organic synthesis. Variable and tunable acidity, from basic through neutral to acidic, allows for some very subtle changes in transition metal coordination chemistry [53,54]. The melting points of [EMIM]Cl/$AlCl_3$ mixtures can be as low as –90 °C, and the upper liquid limit almost 300 °C.

2.2 IONIC LIQUIDS AS CORROSION INHIBITORS

A corrosion inhibitor is a chemical compound that, when added in minute concentration to a liquid or gas decreases the corrosion rates of a material, typically a metal or an alloy [46].
Ionic liquids are a group of corrosion inhibitors which have the following advantages:

- Thermally and hydrolytically stable.
- They are good solvents for a wide range of both inorganic and organic materials.
- Nonflammable and non-corrosive
- No measurable vapour pressure
- Tenable viscosity and electrochemical window
- They are often composed of poorly coordinating ions, so they have the potential to be highly polar yet non-coordinating solvents.
- Ionic liquids are nonvolatile, hence they may be used in high vacuum systems and eliminate many containment problems. They do not evaporate.
- They are immiscible with a number of organic solvents and provide a non-aqueous polar alternative for two-phase systems.

Therefore, ionic liquids provide a useful extension to the range of solvents that are available for synthetic chemistry. Until recently, room-temperature ionic liquids were considered to be rare, but it is now know that many salts form liquids at or close to room temperature [48, 49].There are two basic methods for the preparation of ionic liquids: metathesis of a halide salt with silver, group 1 metal or ammonium ion and acid-base neutralization reactions.

The most common salts in the use are those with alkylammonium, alkylphosphonium, N-alkylpyridium and N, N-1-dialkylimidozoliumcations. The process of adsorption of inhibitors to a metal creates a film of the adsorbate on the surface of the adsorbent. Adsorption is the

adhesion of atoms, ions or molecules from a gas, liquid, or dissolved solid to a surface. Adsorption process between the inhibitor and the metal adopts the following pattern:

$$IL_{(sol)} + nH_2O_{(ads)} \longrightarrow IL_{(ads)} + nH_2O_{(sol)} \quad (5)$$

The efficiency of the ionic liquid shows the ability to be absorbed on the metal surface by displacing the water molecule from the interface which is affected by corrosion [18].
The adsorption of an inhibitor protects the metallic surface and hence the rate of corrosion is reduced [50, 51].

Abdul *et al* [55] investigated the adsorption and corrosion inhibition of mild steel in hydrochloric acid by N-[morpholin-4-yl (phenyl)methyl] benzamide. They used the following materials: Mild steel strips with the composition of 100% aluminium and size of 4 x 1 x 0.025cm. The weight loss was monitored during the experiment as well as the effect of metal as temperature changes. Mild steel cylindrical rods of the same composition embedded in araldite with exposed area of $1cm^2$ we used for potentiodynamic polarization and impedance measurements. The electrode was polished using a sequence of emery papers of different grades and then degreased with acetone. N-[morpholin-4-yl (phenyl) methyl] benzamide was synthesized, purified and characterized by IR and NMR spectroscopy. The concentration of inhibitor ranges from 10^{-2}M to 10^{-7}M. The acid solution was prepared of analytical grade 37% HCl with double distilled water. All tests were conducted at different temperatures in magnetically stirred solutions. For weight loss measurements, each run was carried out in a glass vessel containing 100 ml test solution. A clean weighed steel rod (4 x 1 x 0.025cm) was completely immersed at inclined angle in the solution. The temperature of the solution was maintained at 30±1°C. After 2 hours of immersion, the electrode was withdrawn, rinsed with doubly distilled water, dried thoroughly and weighed. The weight loss was then used to calculate the corrosion rate (CR) in miles per year (mpy) [56].

Saliyan and Dhikari [57] investigated a corrosion inhibitor, N–(3,4–dihydroxybenzyldiene)-3-{8-[trifluoromethyl)quinolin-4-yl]thio}propanohydrazide (DHBTPH) which was synthesized, characterized and tested as a corrosion inhibitor for mild steel in HCl (1M, 2M) and H_2SO_4 (0.5M , 1M) solutions using weight loss method, electrochemical impedance spectroscopy (EIS) and potentiodynamic polarization methods PDP). These results showed

that DHBTPH is a very good inhibitor for mild steel in acidic media. The inhibition efficiency in different acid media was found to be in the decreasing order of 0.5M H_2SO_4 > 1MHCl > 1M H_2SO_4 > 2M HCl. The inhibition efficiency increases with increasing inhibition concentration and with increasing temperature and acted as an anodic inhibitor. Thermodynamic and activation parameters revealed that the inhibition of corrosion by DHBTPH is due to the formation of chemisorbed film on the metal surface. Absorption of DHBTPH was found to follow the Langmuir's absorption isotherm. Chemisorption mechanism was proposed. The mild steel samples were also analyzed by scanning electron microscope (SEM) and concluded that corrosion does not occur in the presence of an inhibition and hence corrosion was inhibited strongly when the inhibitor was present in the acid media.

Scendo and Uznanska [58] studied the inhibition effect of 1-butyl-4-methylpyridium tetrafluoroborate on the corrosion of copper in phosphate solutions.1-Butyl-4-methylpyridium tetrafluoroborate ($4MBPBF_4$) was dissolved at concentrations in the range of 1.0-50.0mM in 0.5M H_3PO_4. The electrode potentials were measured and reported. The scanning electron microscope was used to study morphology of the copper surface in the absence and presence of the inhibitor. Their investigation concluded that the decrease in current densities could be attributed to the decrease in the phosphate ions attack on the copper surface due to the absorption of the inhibitor molecules at the copper/solution interface. The corrosion density decreased when the concentrations of 1-butyl-4-methylpyridinium tetrafluoroborate were increased for both solutions of pH 2 and 4. This indicated the inhibiting effect of $4MBPBF_4$ on corrosion copper.

The addition of 1-butyl-4-methylpyridinium tetrafluoroborate to the phosphate solutions produced higher R_p (Polarization Resistance) values than the blank solutions indicating the formation of a protective layer on the electrode surface. Hence, the polarization resistance values increased with an increase in the concentration of 4MBPBF4 for both solutions of pH2 and 4. In the presence of 1-butyl-4-methylpyridium tetrafluoroborate solution of pH2 and pH4, the inhibition efficient increased with an increase in the concentration of inhibitor. The corrosion rate of copper was significantly reduced as a result of the reduction in the corrosion circuit densities. The protective layer on surface of metal caused the corrosion rate to

diminish in case of less acid solution of phosphate. The scanning electron microscope showed that in the presence of the inhibitor, the film precipitates on the surface of copper. The corrosion current density increased and inhibition efficiency decreased with increasing temperature. The thermodynamic functions of corrosion indicated that 1-butyl-4-methylpyridium tetrafluoroborate absorbed out the copper surface by a physisorption based mechanism involving a spontaneous and exothermic process.

2.3 IMPORTANCE OF USING QUANTUM CHEMICAL METHODS IN THE STUDY OF CORROSION INHIBITORS

Quantum chemical methods can be utilised to understand the mechanism of interaction between the inhibitor and the metal surface. Previous studies have shown that quantum chemical methods can provide an explanation on the interaction mechanism where it is difficult to obtain such data from experimental techniques. Density functional theory and molecular dynamic simulations are the recent approaches involved in computation chemistry. These methods can reveal unrecognised connections between structure and properties. It is from this structure, property relationship where new inhibitors can be designed and developed [59]. The advancement of this relationship between corrosion inhibitor and computation methods have reached a point where the organic molecules of the inhibitor can be correlated directly with the theoretical parameters [60]. Quantum chemistry is a branch of theoretical chemistry which applies quantum mechanics and quantum field theory to address problems in chemistry [61]. Quantum mechanics deals with physical phenomena at nanoscopic scales when the action is on the order of the Planck constant, whereas quantum field theory (QFT) is a theoretical frame work for constructing quantum mechanical models of subatomic particles in particle physics and quasiparticles in condensed matter physics [62, 63]. This field is related to chemistry and physics, and also caters for fields such as atomic physics, molecular physics and physical chemistry, and mathematically it describes the fundamental behaviour at the molecular scale [59, 63]. Therefore all chemical systems can be described using this theory. Also, simplest chemical system can be investigated in purely quantum mechanical terms. In quantum mechanics the physical state of a particle can be expressed as the sum of two operators, one corresponding to kinetic energy the other to potential energy [64].

2.3.1. ELECTRONIC STRUCTURE

Electronic structure is a state of motion of electrons in an electrostatic field created by stationary nuclei [64]. These electrons carry particular energies and have a specific wave function. When quantum mechanical equations are solved, an electronic structure can be obtained.

2.3.2 VALENCE BOND THEORY

Chemical bonding uses two quantum mechanical descriptions namely, valence bond theory and molecular orbital theory. In valence bond theory there is an overlap of two atoms that forms a covalent bond and a pair of electrons is formed between the two atoms. This overlap of two atoms, create a region whereby the probability of finding an electron becomes high. Both atoms are attracted by electrons that are found between them [65].

2.3.3 MULTIPLE BONDS

Multiple bonds are bonds formed from double and triple bonds. These bonds can also experience an overlap, this overlap occurs between the atoms of the double bond. The double bond can consist of one sigma bond (θ) and one pi bond (π) [66].

2.3.4 PI BOND

A bond formed by the sideways overlap of two parallel orbitals. Pi bonds result from the concentration of electron density above and below axis and exhibit binodal planar symmetry [65].

2.3.5 SIGMA BOND

The covalent bond formed due to overlapping of atomic orbital along the inter nucleus axis. It is a stronger and cylindrically symmetrical [65].

2.3.6 QUANTUM CHEMICAL PARAMETERS

Molecular quantities can be defined and enabled using the quantum chemical methods and molecular techniques. The molecular quantities include the shape, the reactivity, the binding properties and the molecular fragments and substituents of a complete molecule. Characterization of compounds can be made on the basis of fragments substituents, whereas

the accountability of the mechanisms is generated in terms of chemical reactivity. These are the use of theoretical parameters of a specific compound [66]. There is a natural overlap between the quantum chemical derived parameters and experimental measured quantities. Experimental measurements have statistical error in quantum derived parameters there, but, generally there is no statistical error in quantum chemical calculations. There is inherent error however associated with the assumptions required to facilitate the calculations. In most cases the direction but not the magnitude of the error is known [65, 66]. In using quantum chemistry –based parameters with a series of related compounds, the Computational error is considered to be approximately constant throughout the series and the prominent quantum chemical parameters can be subdivided as follows: atomic changes, dipole moment(μ), energy and molecular orbital energies [67].

2.3.6.1 ATOMIC CHARGES

Chemical interactions can either be electrostatic or orbital. Electrostatic are polar Chemical interactions whereas orbitals are covalent Chemical interactions. Molecules have an electric charge that is responsible for electrostatic interactions. There are many chemical reactions and physio-chemical properties that are important, and one is the local density or charges, thus, one such based parameter that has been widely employed as chemical reactivity indices, or as measures of weak intermolecular interactions, is the charged based parameters [68].

Despite its usefulness, the concept of a partial atomic charge is somewhat arbitrary, because it depends on the method used to delimit between one atom and the next. As a consequence, there are many methods for estimating the partial charges [69]. Mulliken population analysis is mostly used for the calculation of the charge distribution in a molecule [70]. Quantitative understanding of the structure and reactivity of molecules are easily obtained through the numerical quantities [71]. Also, atomic charges are used for description of the molecular polarity of molecules.

2.3.6.2 MOLECULAR ORBITAL ENERGIES

Other popular quantum chemical parameters include the highest occupied molecular orbital energy and the lowest unoccupied molecular orbital energy. Highest occupied molecular energy is represented by (E_{HOMO}) whereas lowest unoccupied molecular orbital are represented by (E_{LUMO}) [72]. The other names for these orbitals are the frontier orbitals.

These orbitals determine the way the molecule interacts with other species. The HOMO contains electrons and for that reason they are capable of acting as an electron donor, it is their outmost highest energy orbital. The LUMO is the innermost, lowest energy orbital and they could act as the electron acceptor. The formation of a transition state is due to the interaction between the HOMO and LUMO, this is according to the frontier molecular orbital theory [71,72]. The energy of the HOMO is directly related to the ionization potential and the energy of the LUMO is directly related to the electron affinity. The HOMO-LUMO gap i-e the difference i energy between HOMO-LUMO is an important stability index [73]. A large HOMO-LUMO gap implies high stability for the molecule in chemical reactions also other concepts like the activation hardness has been defined at the basis of the HOMO-LUMO energy gap [74]. The qualitative definition of hardness is closely related to the polarization, since there is a decrease of the energy gap that usually leads to earlier polarization of the molecule [75].

2.3.6.3 DIPOLE MOMENT

The most widely used quantity to describe the polarity is the dipole moment of the molecule. Dipole moment is the measure of polarity of a polar covalent bond. It can be defined as the product of charge on the atoms and the distance between the two bonded atoms [75, 76].

2.3.6.4 ELECTRONEGATIVITY

For diatomic molecules, the atom with a net negative charge compared to the other atom, is said to be more electronegative, this is because the qualitative aspects of electronegativity are readily comprehensible. The specification of the electronegativity of an atom, taking into account qualitative aspects, would amount to a specification of its position in an ordinal listing of the elements, such that it would be negative in a diatomic molecule formed with any element listed below it. The criteria for setting up such a list of the atoms in the order of their electronegativity would be the polarity, but not the amount of the partial ionic character of atomic molecules, of which the nuclear quadropole coupling constant is an imperfect measure [77]. The quantitative aspects of electronegativity are less clear. Quantitatively, electronegativity is defined as the tendency of an atom in a molecule to attract electrons [78]. Gordy[79] found a correlation of electronegativity with Zu /r_{cor} where Zu is the effective nuclear change acting on the outermost electrons, and r_{cor} is the covalent radius of the atom.

This correlation between Zu and r_{cor} was a demonstration he took to show that the physical quantity corresponding to the term electronegativity was the potential due to the partially screened nuclear charge at the covalent radius . Other correlation has been made with powers of r. These correlations included the Mulliken's value [80], that the electronegativity represents average of a property over a range of ionization instead of being solely a property of the neutral atom [80, 81]. Alfred and Rochow[82] also found a good correlation of electronegativity with Z^*/r_{cor}^2 and they indicated that the electronegativity represented a force on the atomic electrons at the covalent radius [82, 83].

2.3.6.5 MULLIKEN ELECTRONEGATIVITY

In 1811, J.J Berzelius proposed the concept of electronegativity (c) which later played the major role in modern chemistry because it can be considered as one of the most important chemical descriptors in order to account for the tendency of the atoms to build up a molecular system [84]. About 70 years ago, Pauling introduced an electronegativity scale, by ingenious mixing of thermodynamical and quantum mechanical argument, which has enriched the concept of atomic periodic properties. Further progress was made in 1934 and 1935 by Mulliken, who introduced a different formulation in terms of two other periodic properties, namely the ionization potential and the electron affinity, and enabled the extension of this concept to molecules [74]. The electronegativity definition was subsequently modified and enriched toward a quadral appreciation of the various complexities involved in the concept [85-87]. In a continuous effort to better define the other initiative concept of electronegativity the Parr idea to define as the negative of the chemical potential of the density functional theory (DFT) of Hohenberg and Kohn, i.e. as the first derivative of the energy functional, the connection between electronegativity and quantum mechanics has been established [88-90].

2.3.7 THEORETICAL METHOD

2.3.7.1 DENSITY FUNCTIONAL REACTIVITY INDICES BACKGROUND

Among the chemical concept that has found rigorous quantitative definitions in the framework of the DFT a special attention was given to the electronegativity formulation [88]. For an N- electronic system placed into an external potential V (r), the general (first order) equation of the change in the chemical potential $\mu = \mu[N, V(r)]$ can be written as [70]:

$$d\mu = 2\eta dN + \int f(r) dV(r) dr \qquad (6)$$

where the variation of the chemical potential and the electronegativity is shown in the Parr definition as $\mu = -\chi$

For an electronic system is concluded with variation of the number of electrons and of the external potential through the chemical hardness η:

$$2\eta = \left(\frac{\partial \mu}{\partial N}\right)_{V(r)} \qquad (7)$$

And the Fukui function $$f(r) = \left(\frac{\delta \mu}{\delta V(r)}\right)_N \qquad (8)$$

The chemical potential or the electronegativity concept appears to be strictly connected with the other two, chemical hardness and the Fukui function, in regards to their reactivity criteria. It is not worthy that although in the original hardness definition the factor ½ was put in to make it symmetrical with respect to the chemical potential definition (27), nowadays the convention without this factor is also used (28) in a similar way (see equation 6). The total energy for the electronic system, E= E [N, V(r)] [89] can be written as:

$$dE = \mu dN + \int \rho(r) dV(r) dr \qquad (9)$$

where the chemical potential and the electronic density $\rho(r)$ are defined as:

$$\mu = \left(\frac{\partial E}{\partial N}\right) V(r) \qquad (10)$$

$$\rho(r) = \left(\frac{\delta E}{\delta V(r)}\right)_N \qquad (11)$$

The equation 9 can be rewritten in terms of the Maxwell identities as:

$$\left(\frac{\delta \mu}{\delta V(r)}\right)_N = \left(\frac{\partial \rho(r)}{\partial N}\right)_{V(r)} \qquad (12)$$

Using the Parr definition of electronegativity for the chemical potential, from equation 5 this chemical descriptor takes the form

$$\chi(N) = \left(\frac{\partial E}{\partial N}\right)_{V(r)} \qquad (13)$$

Furthermore, using the same equation (10) incorporate in the hardness definition *e*, the expression for the hardness as the second order derivative of the total energy with respect to the total number of electrons, assumes the form [87,88]

$$\eta(N) = 1/2\left(\frac{\partial^2 E}{\partial N^2}\right)_{V(r)} \qquad (14)$$

Turning now to the Maxwell identity equity the Fukui index given by equation can be defined in terms of the density and the number of electrons as

$$f(r) = \left(\frac{\partial \rho(r)}{\partial N}\right)_{N(r)} \qquad (15)$$

Combining in the equation, the expression 7 and 10, the following differential equation for the electronegativity is obtained [89, 90, 91]

$$d\chi = \left(\frac{\partial \chi}{\partial N}\right)_{V(r)} dN - \int\left(\frac{\partial \rho(r)}{\partial N}\right)_{V(r)} dV(r)dr \qquad (16)$$

Taking into account the relation 7 expressed within the Parr electronegativity definition

$$\left(\frac{\partial \rho(r)}{\partial N}\right)_{V(r)} = \left(\frac{\delta \chi}{\delta V(r)}\right)_N \qquad (17)$$

It is easily recognised that equation 11 has the same form as equation 6 and 9 however; in order to find the electronegativity we propose the alternative integrations of equation 1 in the following way. First let us express the hardness and Fukui function through the relations (22)

$$2\eta = 1/S \tag{18}$$

$$f(r) = \left(\frac{S(r)}{S}\right) \tag{19}$$

where S and S(r) represent the global and local softness defined as

$$S = \left(\frac{\partial N}{\partial \mu}\right)_{V(r)} \tag{20}$$

$$S(r) = \left(\frac{\partial \rho(r)}{\partial \mu}\right)_{v(r)} \tag{21}$$

Assuming that

$$N = \int_{-\infty}^{+\infty} \rho(r)dr \tag{22}$$

The connection between the global and the local softness indices can be obtained:

$$S = \int_{-\infty}^{+\infty} S(r)dr \tag{23}$$

Applying to the exact formula of Bekowitz and Parr and Ayer relatively the conventional linear response function [90, 91], $[\delta\rho(r)/\delta V(r')]_N$ with softness, local softies and local softies kernel, the three quantum mechanical constraint such as the translational invariance condition , the Hellman – Feyman theorem and the normalization of the linear response function, the softness Kernel S (r, r')

$$S(r,r') = L(r')\delta(r-r') + \rho(r)\rho(r') \tag{24}$$

As a sum of local and non- local contributions now, the local response function:

$$L(r) = \frac{\nabla\rho(r)}{\nabla V(r)} \tag{25}$$

Corresponds to the scalar quantity

$$-\nabla\rho(r).\nabla V(r)//\nabla V(r)|^2 \qquad (26)$$

This model is general besides the different ways to evaluate the non-local term in equation 19

Integrating the equation 19 over r' relating 16 for the local softness becomes :

Equating, $$S(r) = L(r) + N\rho(r) \qquad (27)$$

And when the relations of 17 and 18 are used, the corresponding global softness becomes: {17}

$$S = \int_{-\infty}^{+\infty} L(r)dr + N^2 \qquad (28)$$

All these chemical descriptions depend on the electronic density. Hence they are derived to combine with Mulliken electronegativity [80].

CHAPTER 3

EXPERIMENTAL DETAILS

3.1 Materials

- Mild Steel (MS) having composition (wt.) C = 0.17, Mn = 0.46, Si = 0.26, S = 0.017, P = 0.019, and balance Fe were used for electrochemical studies.
- An aggressive solution of hydrochloric acid (AR grade) of 1 M concentration was used for all the experiments.

3.2 Reagents

The hydrochloric acid used for this study was obtained from MERCK CHEMICALS.

3.3 Inhibitors Used

- ILs $[BDMIM]^+$ $[BF_4]^-$, $[EMIM]^+$ $[BF_4]^-$, $[BMPy]^+$ $[Br]^-$ and $[EMPy]^+$ $[Br]^-$ were purchased from Sigma Aldrich with mass fraction purity > 97% and were used without any further purification. All the chemicals were stored over 0.4 nm molecular sieves to remove moisture.
- Aggressive solutions of 1 M HCl, were prepared with AR grade 32% HCI in distilled water.
- The stock solutions of ionic liquids were diluted to a certain concentration of inhibitor.
- The inhibitor concentrations prepared were 50, 100, 300 and 500 ppm and the electrochemical studies were performed.

3.4 Electrochemical Measurements

A three-electrode cell were used such as Mild steel as working electrode (WE), Platinum as counter electrode (CE), Saturated calomel with Ag/ AgCI as a reference electrode (RE).
All the Experiments were carried out at atmospheric condition without stirring.

- Prior to the electrochemical measurement, a stabilization period of 30 min was allowed, which was proved to be sufficient to attain a stable value of E_{corr}.

- The potentiodynamic polarization curves were recorded in the potential range from -250 to +250 mV (SCE) with scan-rate of 1 mV/S. All potentials were measured against SCE.

- The EIS measurements were carried out in a frequency range from 100 kHz to 0.00001 kHz under potentiodynamic conditions, with amplitude of 10 mV peak-to-peak, using the AC signal at E_{corr}.
- Inhibitors are used in the surface treatment of metals to improve the corrosion resistance.

3.5 Potentiodynamic Polarization (PDP)

To get values of corrosion potential (E_{corr}), corrosion current density (i_{corr}), anodic and cathodic Tafel slopes (b_a and b_c), Polar Resistance (RP) and Corrosion Rate, Potentiodynamics was used. The linear Tafel segments of anodic and cathodic curves were extrapolated to corrosion potential to obtain corrosion current densities (i_{corr}). The inhibition efficiency was then evaluated from the measured i_{corr} value using the relationship [92]

$$E_{PDP}\% = \frac{i^{o}_{corr} - i^{i}_{corr}}{i^{0}_{corr}} \qquad (29)$$

where i^{0}_{corr} and i^{i}_{corr} are values of corrosion current density in absence and in presence of inhibitor, respectively.

3.6 Electrochemical Impedance Spectroscopy (EIS)

Electrochemical impedance spectroscopy was used to obtain parameters such as the resistance of charge transfer (R_{ct}), and the capacity of double layer (C_{dl}), and from this obtained parameters, the inhibition efficiency was calculated using the equation below;

$$E_{EIS}\% = \left(1 - \frac{R^{0}{}_{ct}}{R_{ct}}\right) \times 100 \qquad (30)$$

where, $R^{0}{}_{ct}$ is the charge transfer resistance in the absence of the inhibitor and R_{ct} is the charge transfer resistance in the presence of the inhibitor [92,93].

3.7 Quantum Chemical Calculations

Dipole moments (μ) is the measure of net molecular polarity, which is the magnitude of the charge Q at either end of the molecular dipole times the distance r between the charges

$$\mu = Q \times r \qquad (31)$$

Fukui function: The Fukui function, denoted by f(**r**), is defined as the differential change in electron density due to an infinitesimal change in the number of electrons. The nucleophilic and electrophilic Fukui functions can also be calculated using the finite difference approximation as follows; [94]

$$f^{+} = q_{(N+1)} - q_N \qquad (32)$$

$$f^{+} = q_N - q_{(N+1)} \qquad (33)$$

Ionization potential (I) is the amount of energy required to remove an electron from a molecule; it is related to the energy of the E_{HOMO} through the equation:

$$I \cong - E_{HOMO} \qquad (34)$$

Electron affinity (EA) is the energy released when an electron is added to a neutral molecule; it is related to E_{LUMO} through the equation:

$$A \cong - E_{LUMO} \qquad (35)$$

Energy Gap (ΔE): The energy difference between the highest occupied molecular orbital (HOMO) and the lowest unoccupied molecular orbital (LUMO) within a given inhibitor molecule is referred to as energy gap and denoted with a letter ΔE [95].

$$\Delta E = E_{LUMO} - E_{HOMO} \qquad (36)$$

Global Hardness and Softness: Global hardness (η) and softness (σ) are molecular properties that also facilitate the analysis of the molecular reactivity. Soft molecules are more

reactive than hard molecules if electron transfer or rearrangement is necessary for the reaction. Hard molecules resist changes in their electron number and distribution [96].

$$\eta \cong -\tfrac{1}{2} (E_{HOMO} - E_{LUMO}) \quad (37)$$

$$\sigma = 1/\eta \cong -2/ (E_{HOMO} - E_{LUMO}) \quad (38)$$

All Geometry optimizations and quantum chemical calculations were performed using density functional theory (DFT) using the 6-31G(d) basis set. The Becke's Three Parameter Hybrid Functional using the Lee-Yang-Parr correlation functional theory (B3LYP) was selected for the calculations. The DFT method is widely utilized in the analysis of the characteristics of the inhibitor/metal surface mechanisms and in the description of the nature of the inhibitor on the corrosion process. Moreover, DFT/B3LYP is highly recommended for the understanding of chemical reactivity and selectivity in terms of frontier molecular orbitals (the HOMO and the LUMO) and related properties such as polarizability, hardness (η) and electronegativity, electron affinity (EA) and ionization potential (IP). In terms of the Koopman's theorem. Schematic structures were drawn using the ChemOffice package in the UltraChem 2010 version while optimized structures were drawn using the Spartan 10 V1.01 program. The quantitative structure activity relationships plots and the corresponding equations were derived using the xlstart program [92, 94, 95, 97].

CHAPTER 4

RESULTS AND DISCUSSION

4.1 Electrochemical measurements

4.1.1 Potentiodynamic polarization (PDP)

Potentiodynamic polarization curves were recorded for mild steel in 1 M HCl in the absence and presence of different concentrations (100 – 500 ppm) of the studied ionic liquid inhibitors and the results are presented in Figures 4.1 – 4.4. The values of corrosion potential (E_{corr}), corrosion current density (i_{corr}), anodic and cathodic Tafel slopes (b_a and b_c), polarization resistance (R_P) and corrosion rate obtained from the fitting of the polarization curves are presented in Table 4.1. The linear Tafel segments of anodic and cathodic curves were extrapolated to corrosion potential to obtain corrosion current densities (i_{corr}). The inhibition efficiency was evaluated from the measured i_{corr} value using the relationship below;

$$E_{PDP}\% = \frac{i^{o}_{corr} - i^{i}_{corr}}{i^{0}_{corr}} x\,100 \qquad (29)$$

where i^{0}_{corr} and i^{i}_{corr} are values of corrosion current density in absence and in the presence of inhibitor, respectively.

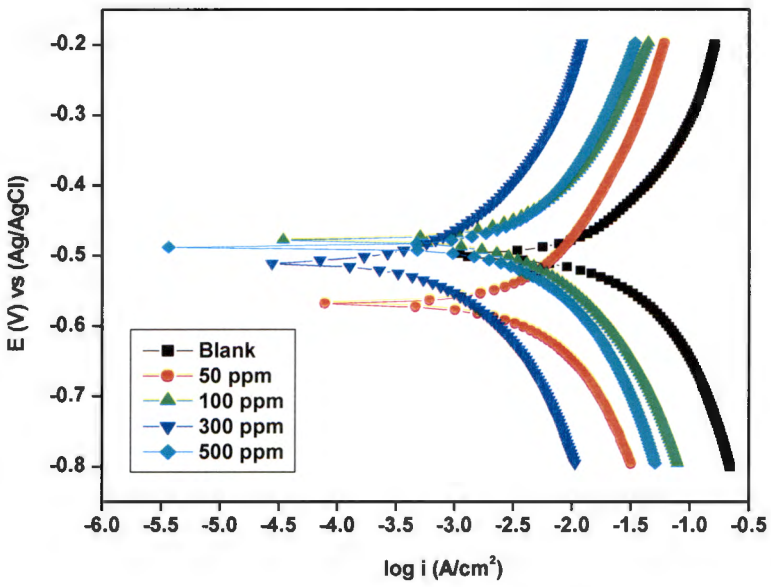

Figure 4.1: Potentiodynamic polarization curve for mild steel in 1 M HCl in the absence and presence of different concentrations of $[BDMIM]^+$ $[BF_4]^-$.

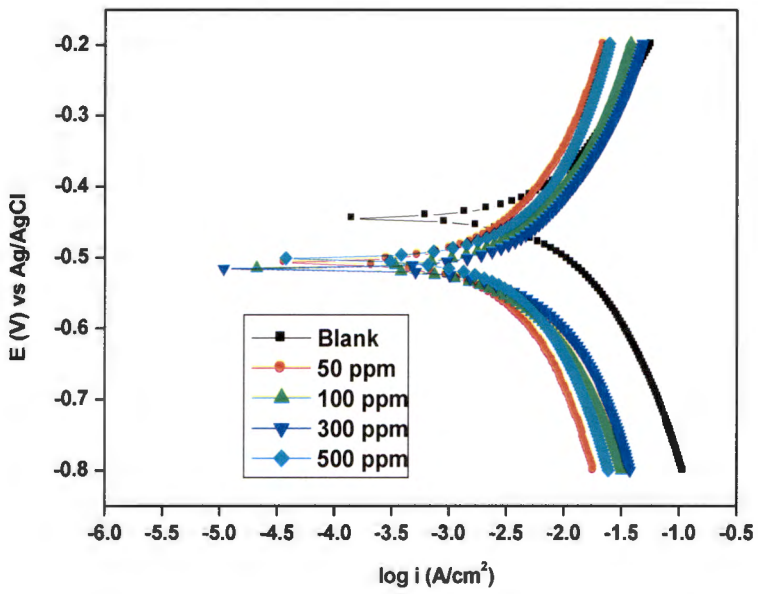

Figure 4.2: Potentiodynamic polarization curve for mild steel in 1 M HCl in the absence and presence of different concentrations of $[EMIM]^+$ $[BF_4]^-$.

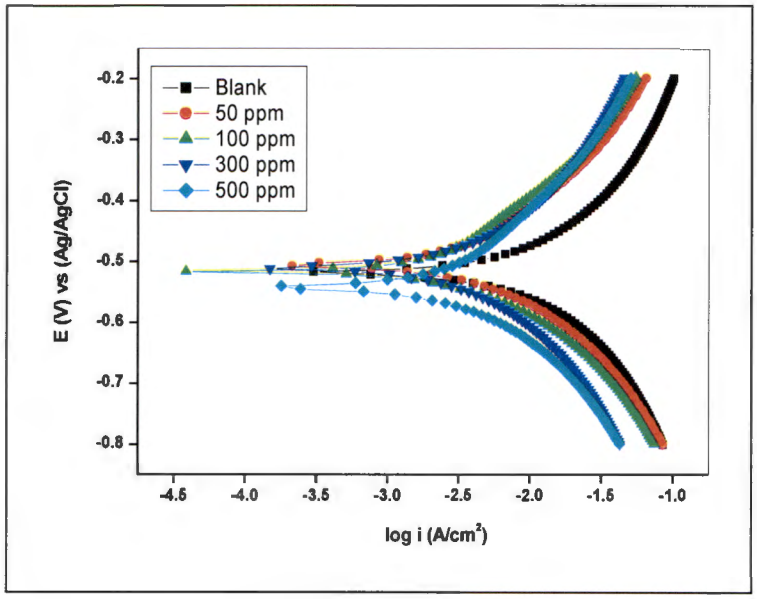

Figure 4.3: Potentiodynamic polarization curve for mild steel in 1 M HCl in the absence and presence of different concentrations of $[BMPy]^+$ $[Br]^-$.

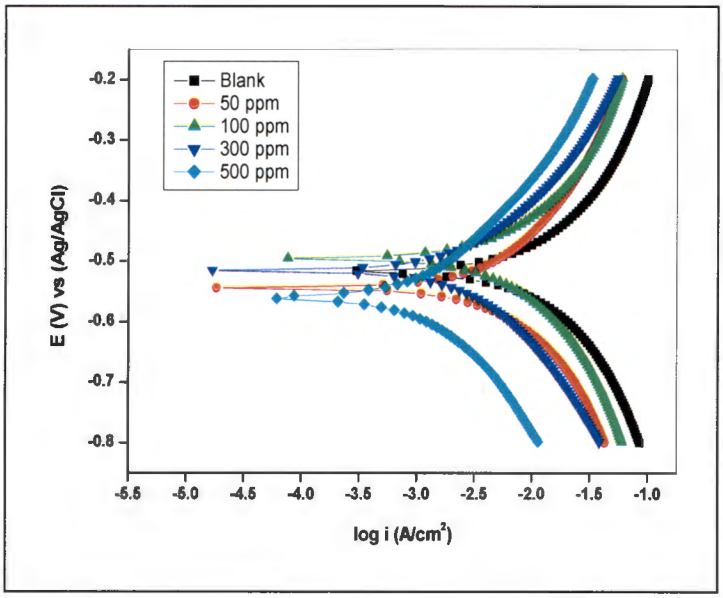

Figure 4.4: Potentiodynamic polarization curve for mild steel in 1 M HCl in the absence and presence of different concentrations of $[EMPy]^+$ $[Br]^-$.

The values of parameters such as E_{corr}, I_{corr}, Tafel constants % *a* (anode slope) and % *c* (cathode slope), R_p, and corrosion rate were also determined from Tafel analysis. The potentiodynamic polarization measurements provided an assessment of corrosion behaviour under dynamic conditions. The measurements were instantaneous and provided rapid measurement of reactions involving rapid electron transfer. The relative corrosion behaviour was determined by the differences in concentrations. It is expected that from classic corrosion theory, the lower pH of the aqueous solutions causes a right shift in the Tafel plots, directly increasing I_{corr} with increase in the acidity [98]. This means that, the more you increase the concentration in acidic medium, the more value of I_{corr} increases. It is evident from the results that, in the presence of the inhibitor, the curves are shifted to the lower current region. This trend shows and confirms the inhibition ability of the ionic liquid corrosion inhibitors utilized in this study.

Polarisation curves display a shift to lower current regions as a result of the inhibitor. The corrosion potential is the potential at which the rate of oxidation of M, is equal the rate of reduction of H^+; this is the only point in this system where the total rates of oxidation and reduction are equal and that is at the intersection represented by a "mixed" (inhibit both the anodic dissolution and cathodic hydrogen evolution reaction) or corrosion potential E_{corr}. These definitions assist in determining further that, an inhibitor can be regarded as an anodic or cathodic when E_{corr} is greater than 85 mV. It is from this information that we observe that a shifting of the curves occurs in the cathodic region and the ILs in the study behaves as mixed type inhibitors. [99, 100]. The slight change in the values of β_a and β_c upon addition of the inhibitors when compared with the blank suggests that the ILs get adsorbed onto the metal surface without affecting the mechanism of the mild steel corrosion in the acid . The higher values of β_c compared to the values of β_a suggests predominant cathodic reactions and hence, the inhibitors will have more effect on the cathodic reaction sites [101].It can be observed that the current density (i_{corr}) decreases as the concentration of inhibitors increases, which confirms the corrosion inhibition activity of the studied ILs. The inhibition efficiency increases with increase in concentration of the inhibitors with a maximum value of 90.84% obtained for $[BDMIM]^+[BF_4]^-$ as shown in Table 1.

The plots of *%IE* obtained from the potentiodynamic polarization study *versus* concentration of inhibitors are shown in Figure 5. The *%IE* at 500 ppm follows the order $[BDMIM]^+[BF_4]^-$ > $[EMPy]^+[Br]^-$ > $[BMPy]^+[Br]^-$ > $[EMIM]^+[BF_4]^-$. It can be observed from table that the values of inhibition efficiency ranging from 50ppm – 500ppm are almost close to each other.

The following aspects about ILs should be taken into account, and that is solvatophobic interactions are present between ILs and the hydrocarbon portion of the surfactants, thus leading to the possibility of formation of surfactants micelles in ILs and enhancing the solvation characteristics of the (ILs +Surfactants) systems. [102,103]. Also, the inherent amphilic nature of some cations, e.g. RNH_3^+., leads us to anticipate that, in aqueous solution, interfacial and aggregation phenomena should become an important issue that ultimately can drive micelle formation with specific structure, shape and properties. With the possibility of fine tuning the hydrophobicity of ionic liquids by changing the alkyl chain length, the type of head group, and/or the nature and the size of the counter ion, one can affect both the structure and these micelle aggregates. This can lead to the modification of their major characteristics such as the critical micelle concentration (cmc), and the aggregate number. [102]It is in such cases, this particular aspect allow us to consider ionic liquids (when dispersed in aqueous solution) as a new class of surfactant with new abilities. In this regard, along with the catalytic effect that ionic liquids can possess by themselves, the appearance of aggregated ionic liquids dispersed in the solvent provides the possibility of combining, to some extent, two reactants completely different in nature (hydrophilic and hydrophobic) into a macroscopically homogenous solution[103].

This observation in the trend of inhibition efficiency with change in concentration of ILs is not impossible and can be attributed to self-aggregation. Surface active compounds such as ILs and surfactants have been reported to exhibit higher corrosion inhibition potential in their aggregated or micelle forms [104,105]. The higher *%IE* obtained for $[BDMIM]^+[BF_4]^-$ (at 500 ppm) compared with other ILs considered in this study can be attributed to the $[BF_4]^-$ in the cluster HOMO which is a cation based $MO.BF_4^-$ is symmetrical, the negative charge is distributed equally over several atoms, and it is composed of highly electronegative fluorine atoms. As compared with Br^-, which is less electronegative, the higher the electronegativity of a metal the less likely it is to corrode (i.e. they show corrosion resistance on metal). Metals

that corrode easily have a low electronegativity and therefore ILs with $[BF_4]^-$, tends to be preferred corrosion inhibitors. It has also been observed that adsorption depends mainly on certain physico-chemical properties of the inhibitor group, such as electron density at the donor atom, π-orbital character, and the electronic structure of the molecule.

In the structure of the imidazolium bases, the atoms of the imidazolium and the –C=N- group can form a big π bond. Then, not only can the π electron of the imidazolium bases enter unoccupied orbitals of iron, but the π^* orbital can also accept the electrons of d orbitals of iron to form feedback bonds, then produce more than one centre of adsorption action[106]. Meanwhile, the presence of the electron donating group on the imidazolium base structure (F), increases the electron density on the nitrogen of the –C=N group, resulting in high inhibition efficiency. Therefore, $[BDMIM]^+[BF_4]^-$ is a better inhibitor than other ILs under study in the corrosion of mild steel in 1 M HCl.

Table 4.1: Potentiodynamic polarization parameters such as corrosion potential (E_{corr}), corrosion current density (i_{corr}) and anodic and cathodic Tafel slopes (βa and βc) using different inhibitors.

Concentration	$-E_{corr}$ (mV)	i_{corr} (mA/cm^2)	b_a (mV/dec)	b_c (mV/dec)	*IE%*
Blank	518	10310	131	135	-
		$[BDMIM]^+[BF_4]^-$			
50 ppm	574	2849	139	183	72.36
100 ppm	483	2563	114	158	75.14
300 ppm	515	2125	154	167	79.38
500 ppm	493	944	88	120	90.84
		$[EMIM]^+[BF_4]^-$			
50 ppm	507	2970	352	288	71.19
100 ppm	516	2838	208	212	72.47
300 ppm	511	2541	145	164	75.35
500 ppm	503	2275	103	102	77.93
		$[BMPy]^+[Br]^-$			

50 ppm	505	2525	112	154	75.50
100 ppm	516	2100	111	179	79.63
300 ppm	506	2066	130	136	79.96
500 ppm	542	1977	111	180	80.82
		$[EMPy]^+[Br]^-$			
50 ppm	545	3110	147	121	69.80
100 ppm	397	3078	188	167	70.14
300 ppm	516	1551	141	137	84.95
500 ppm	562	1268	130	154	87.70

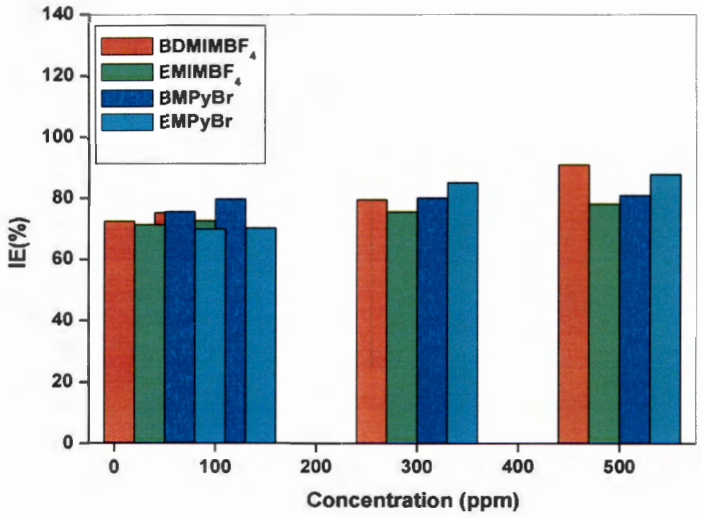

Figure 4.5: Inhibition Efficiency versus concentration from the Potentiodynamic polarization

4.1.2 Electrochemical Impedance Spectroscopy (EIS)

After carrying out the impedance measurements on mild steel in 1 M HCl with and without inhibitors at various concentrations; the Nyquist, Bode impedance and phase angle plots were obtained, and are presented on Figures 4.6- 4.9. The Nyquist plots exhibit single depressed capacitive arc over the frequency range studied, corresponding to one time constant in the Bode plots. EIS methods provide information about the kinetics of the electrode processes as well as the surface properties of the investigated system. Also, with the single experimental

procedure encompassing a single experimental broad range of frequencies the influence of the governing physical and chemical phenomena may be isolated and distinguished at a given applied potential. It has found widespread application in the field of characterization of material and in corrosion phenomena [107, 108].

Electrochemical impedance is usually measured by applying an AC potential to an electrochemical cell and then measuring the current through the cell. Assume that we apply a sinusoidal potential excitation. The response to this potential is an AC current signal. This current signal can be analyzed as a sum of sinusoidal functions (a Fourier series). The plot of the real part of impedance against the imaginary part gives a Nyquist Plot. The advantages of Nyquist Plots is that it gives a quick overview of the data for qualitative interpretation[109].

We also obtain the shape of the curve for making qualitative interpretation of the data. The dissolution of mild steel is therefore controlled by the single charge transfer process, which is not affected by the addition of inhibitor. It is the similarity in the shapes of the Nyquist plots in the absence and presence of inhibitors that reveals that the corrosion mechanism is unaffected by the addition of the ILs.

The increasing diameter of the capacitor loop upon addition of the inhibitors is an indication of corrosion inhibition due to the formation of protective film on the mild steel surface. The impedance modulus of the system also increased with increase in the concentration of the inhibitor. This suggests the formation of protective film on the mild steel surface and consequently reduction in corrosion rate [110,111]. Based on the formation of new phase angle shift, due to formation of protective layer when we increase the concentration, the Nyquist and Bode plots shows the larger diameter of [BDMIM][BF_4], which corresponds to its better inhibition capability, compared to other ILs under study.

The curve fitting and the simulation of the Nyquist and Bode plots was carried out by using the R (RQ) equivalence model circuit shown in the figure 4.10.

The kinetic parameters obtained from the fitting are presented in Table 4.2. The depression in Nyquist semicircles is a feature for solid electrodes and often referred to as frequency depression and attributed to the roughness and inhomogeneity of the solid electrode. In this behaviour of solid electrodes, the parallel network charge resistance double layer capacitance is established where an inhibitor is present. For the description of a frequency independent

phase shift between an applied alternating current (ac) potential and its current response, a constant phase element (CPE) is used. The values of C_{dl} (double-layer capacitance) were calculated using the equation below [112] :

$$C_{dl}(Y_0 R_{ct}^{1-n}) \quad (39)$$

where Y_0 is the CPE (constant phase capacitor) constant, R_{ct} the resistance of the charge transfer and n is a CPE exponent w which can be used as a gauge of the heterogeneity or the roughness of the surface [113].

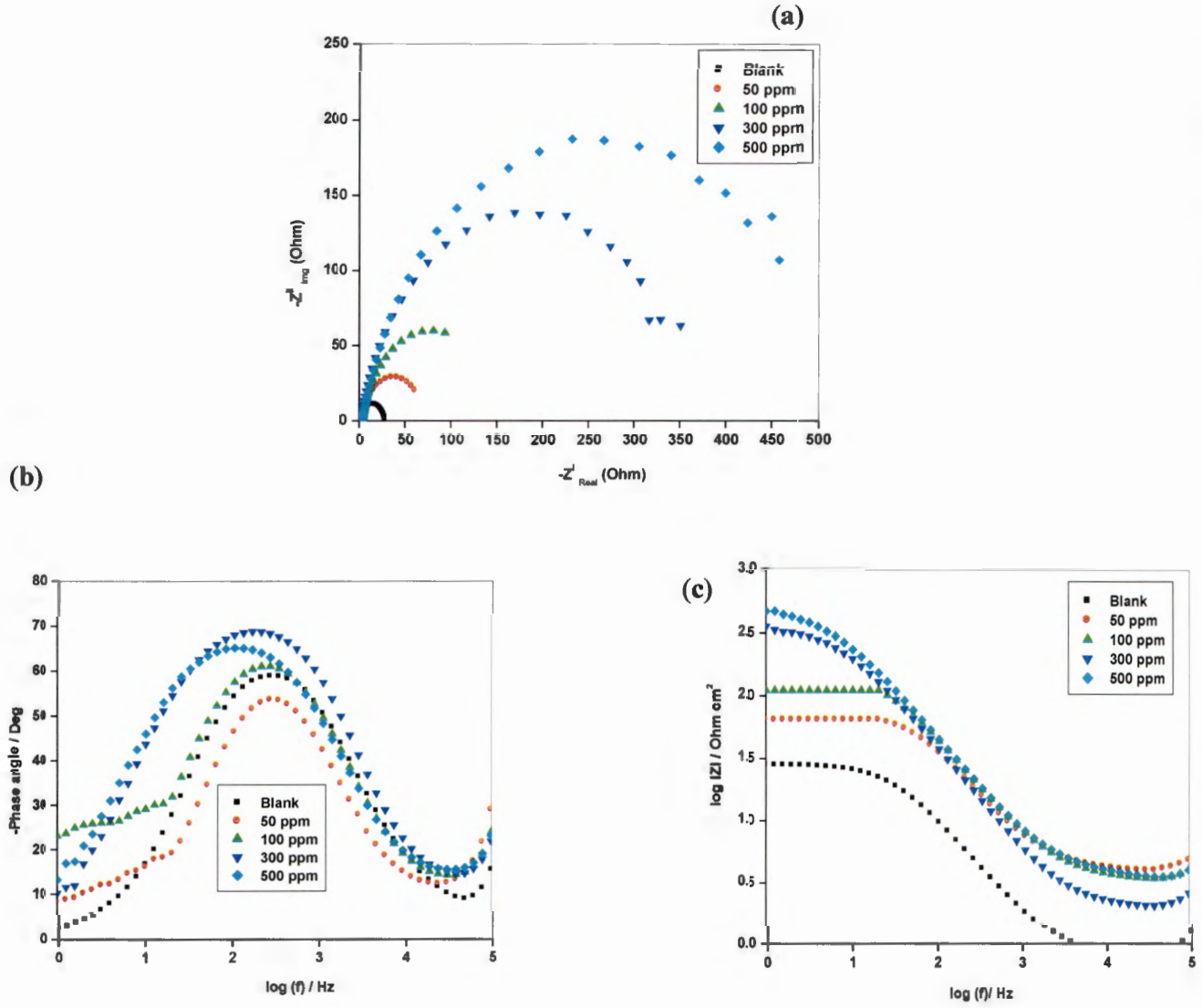

Figure 4.6: (a) Nyquist plot, (b) -Phase angle vs. log f (c) log Z vs. log f of mild steel in 1 M HCl in the absence and presence of different concentrations of **[BDMIM]$^+$[BF$_4$]**

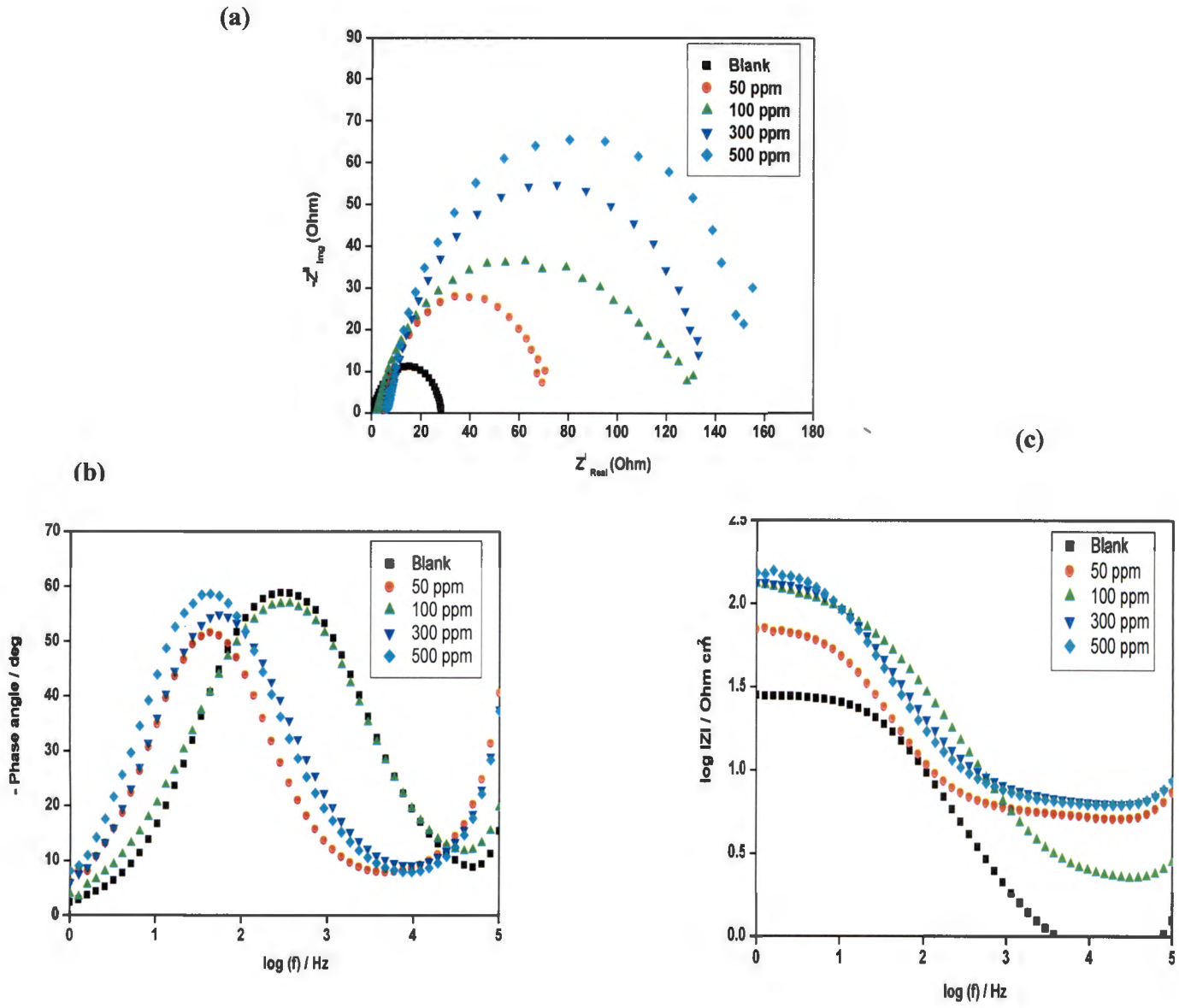

Figure 4.7: (a) Nyquist plot, (b) -Phase angle vs log f (c) log Z vs log f of mild steel in 1 M HCl in the absence and presence of different concentrations of $[EMIM]^+[BF_4]^-$

(a)

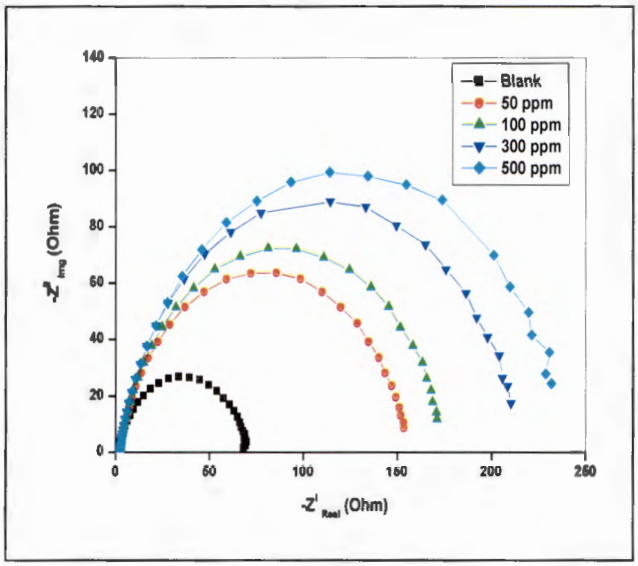

(b)

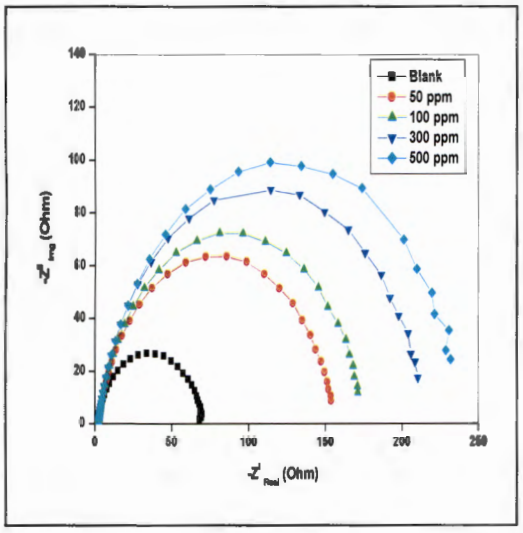

(c)

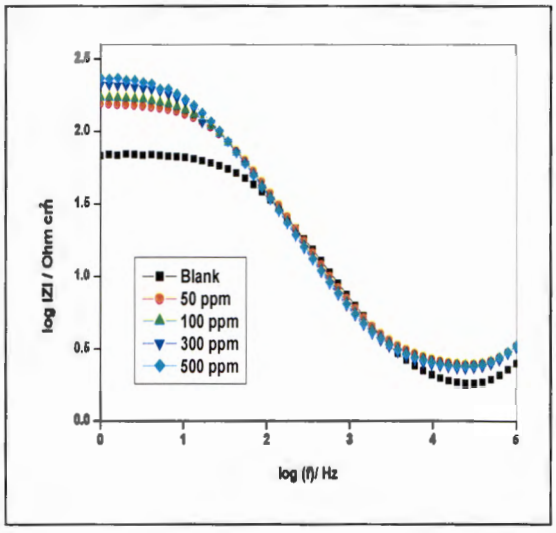

Figure 4.8: (a) Nyquist plot, (b) -Phase angle vs log f (c) log Z vs log f of mild steel in 1 M HCl in the absence and presence of different concentrations of **[BMPy]$^+$[Br]$^-$**

(a)

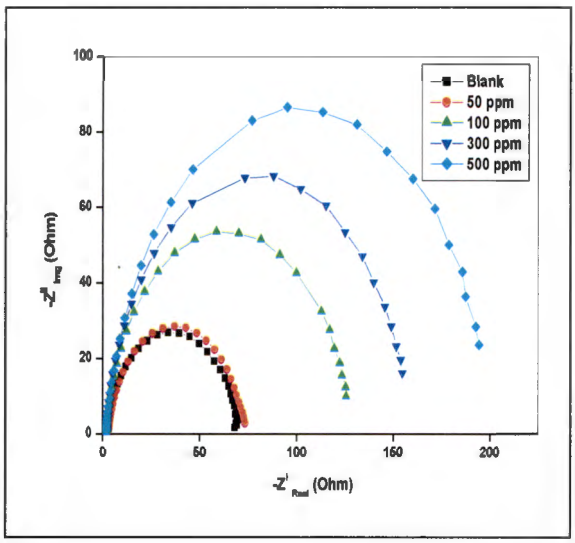

(b)

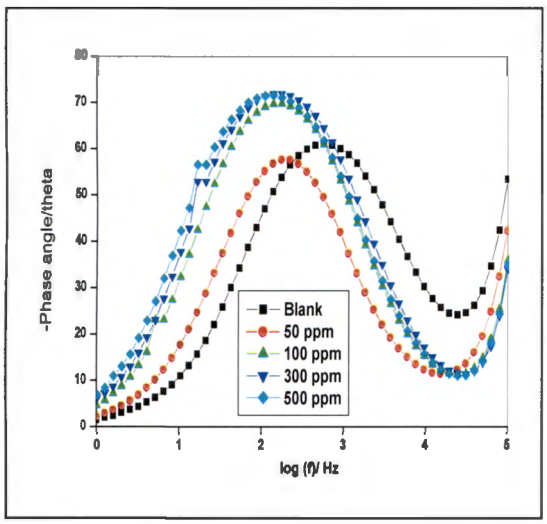

(c)

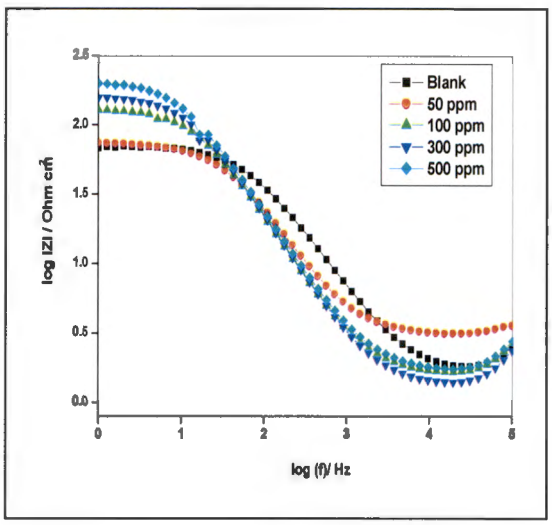

Figure 4.9: (a) Nyquist plot, (b) -Phase angle vs log f (c) log Z vs log f of mild steel in 1 M HCl in the absence and presence of different concentrations of **[EMPy]$^+$[Br]$^-$**

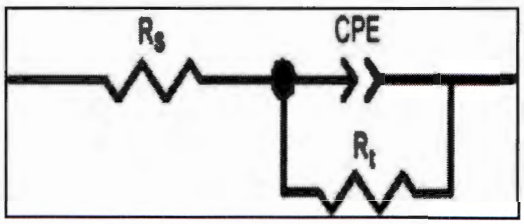

Figure 4.10: The equivalent circuit of the impedance spectra obtained for$[BDMIM]^+$ $[BF_4]^-$, $[EMIM]^+$ $[BF_4]^-$, $[BMPy]^+$ $[Br]^-$ and $[EMPy]^+$ $[Br]^-$

Table 4.2: Electrochemical impedance parameters such as the resistance of charge transfer (R_{ct}), capacity of double layer (C_{dl}), using R_1 (R_2C_1) circuit by different inhibitors.

Concentration of inhibitor (ppm)	R_s (Ω cm^2)	R_{ct} (Ω cm^2)	n	C_{dl} (μF cm^{-2})	IE%
Blank	0.76	28.2	0.80	571.0	-
		$[BDMIM]^+[BF_4]^-$			
50 ppm	5.23	109.1	0.85	437.2	74.15
100 ppm	5.17	122.3	0.85	325.2	76.94
300 ppm	5.95	228.0	0.85	285.8	87.60
500 ppm	5.21	359.0	0.87	227.1	92.14
		$[EMIM]^+[BF_4]^-$			
50 ppm	5.64	88.2	0.87	366.6	68.02
100 ppm	6.13	117.6	0.79	173.3	76.02
300 ppm	6.24	134.6	0.83	162.3	79.04
500 ppm	6.28	160.4	0.86	141.0	82.41
		$[BMPy]^+[Br]^-$			
50 ppm	1.00	71.2	0.85	151.7	60.39
100 ppm	1.66	125.8	0.90	133.8	77.58
300 ppm	1.41	158.2	0.90	131.9	82.17
500 ppm	1.75	201.8	0.89	130.8	86.02
		$[EMPy]^+[Br]^-$			
50 ppm	2.36	161.3	0.86	129.8	82.51
100 ppm	2.31	175.8	0.86	115.7	83.95
300 ppm	2.16	215.8	0.87	107.1	86.93
500 ppm	2.20	239.4	0.87	102.8	88.22

The figures obtained from impedance spectra yield a semi-circular shape which indicates that corrosion of mild steel in 1 M HCl solution is mainly controlled by a charge transfer process. The charge transfer resistance (R_{ct}) corresponds to the resistance between the metal and outer Helmholtz plane and was calculated from the difference in impedance at lower and higher frequencies. To obtain the double-layer capacitance (C_{dl}), the frequency at which the imaginary component of impedance is maximum ($-Z''_{max}$) is found and C_{dl} values are calculated from the following equation [114] :

$$F(-Z''_{max}) = \frac{1}{2\pi C_{dl} R_{ct}} \tag{40}$$

The impedance response to mild steel in HCl changes significantly with increasing inhibitor concentration. In the case of the electrochemical impedance spectroscopy, the inhibition efficiency (IE) is calculated using charge transfer resistance using the following equation;

$$E_{PDP}\% = \frac{i^{o}_{corr} - i^{i}_{corr}}{i^{0}_{corr}} x\,100 \tag{30}$$

as the inhibitor concentartion increases, the R_t values increased, while the C_{dl} values decreases which is due to the adsorption of inhibitor on the metal surface [115].

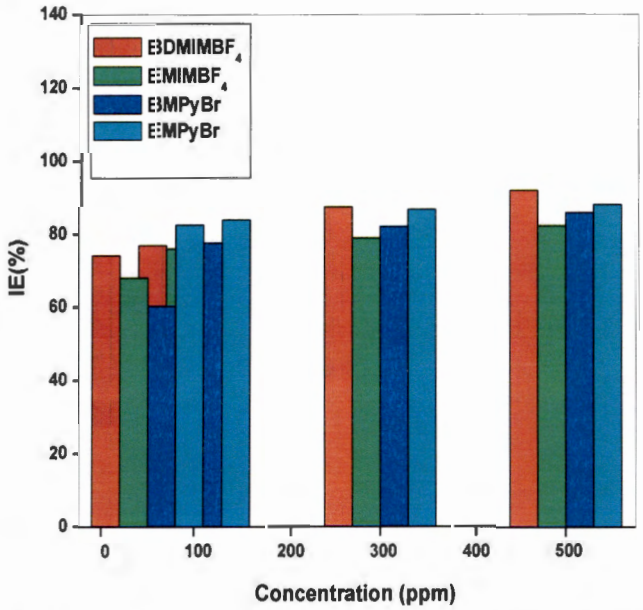

Figure 4.11: Inhibition Efficiency versus concentration from the EIS

4.2 Adsorption Isotherm and Thermodynamic Parameters-

Adsorption isotherms can be used to describe the metal inhibitor interactions. It helps in showing the mechanism followed during the adsorption process between the metal surface and the inhibitor Example of adsorption isotherms includes Frumkin, Freundlich, Temkin, and Langmuir adsorption isotherms.

In this study, Temkin and Langmuir adsorption isotherms were used to determine the inhibitors adsorption equilibrium constant (K_{ads}) from the Tafel polarisation and the EIS data as they gave the best linear fit when applied to the studied inhibitors data.

Langmuir adsorption isotherm which is the plot of concentration of the inhibitor/surface coverage against the concentration of the inhibitor (Eqn 6) gave the best linear relationship for [BDMIM] [BF_4], [EMIM] [BF_4], [BMPy] [Br] and [EMPy] [Br], while Temkin adsorption isotherm which is the plot of surface coverage (θ) against logarithmic of concentration equation 5, gave the best linear relationship for [BDMIM] [BF_4]. In Langmuir adsorption isotherm, surface coverage (θ) of the inhibitor on the mild steel surface is related to the concentration of the inhibitor (C_{inh}) in the bulk solution according to the following equation:[116,]

This equation can be rearranged to be like the equation of a straight line as follows;

$$\frac{C}{\theta} = mC + \frac{1}{K_{ads}} \tag{41}$$

where C is the concentration of the inhibitors, θ the degree of surface coverage, K_{ads} is the equilibrium constant of the adsorption/desorption process and m is the slope. In Eqn 6, C/θ represents the y-axis, C the x-axis, m the slope and $1/K_{ads}$ the intercept on y-axis. For Temkin adsorption isotherm, the following equation was used;

$$\theta = -\frac{1}{2_a}(\ln K_{ads} + \ln C) \tag{42}$$

where θ is surface coverage, K_{ads} Temkin adsorption constant, "a' Temkin parameter, and C is the concentration of the inhibitor. The Temkin parameter was calculated using the following equation;

$$Slope = -\frac{1}{2_a} \tag{43}$$

Then K_{ads} was calculated using the following equation;

$$Intercept = -\frac{1}{2_a} \ln K_{ads} \tag{44}$$

Gibbs free energies of adsorption (ΔG^{o}_{ads}) for the four ionic liquids studied were calculated from the K_{ads} value using the equation below;

$$\Delta G^{o}_{ads} = -RT \ln(55.55 K_{ads}) \tag{45}$$

where ΔG^{o}_{ads} is the Gibbs free energy of adsorption, the value 55.55 is the molar concentration of water in the solution, T is the absolute temperature in Kelvin and K_{ads} is the equilibrium constant for the adsorption process. Negative values of ΔG^{o}_{ads} shows a spontaneous process while positive values indicate non-spontaneous [117].

The Langmuir adsorption plots are presented in Figure 4.12 while the Temkin plot is presented in Figure 4.13. The estimated K_{ads} and Gibbs free energies of adsorption (ΔG^{o}_{ads}) for the four inhibitors studied are presented in Table 4.3. The adsorption plots best fits the Langmuir adsorption model as compared to Temkin, in describing metal inhibitor interaction, as seen by the presentation of the graphs in Figures 4.12 and 4.13

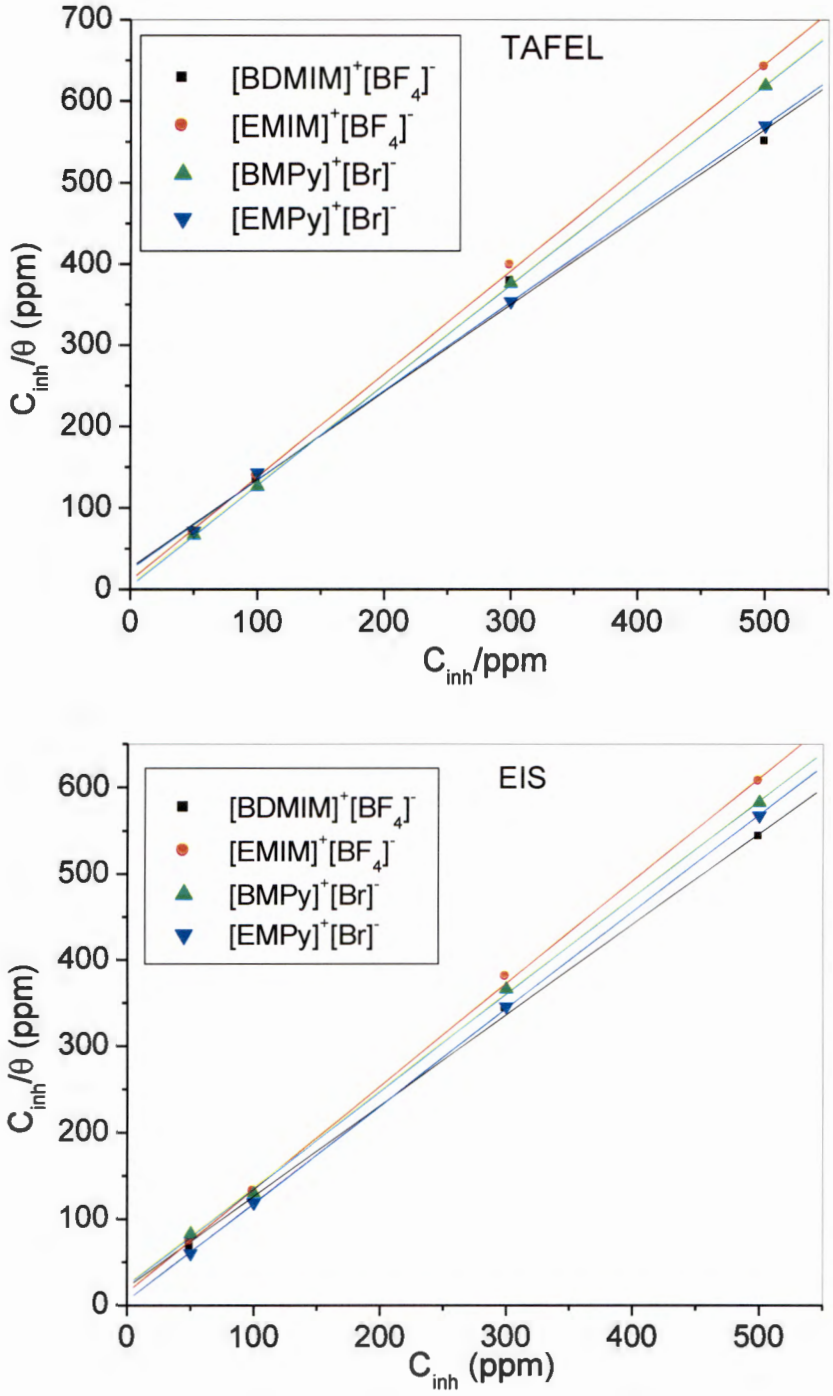

Figure 4.12: Langmuir adsorption isotherm plot for $[BDMIM]^+$ $[BF_4]^-$, $[EMIM]^+$ $[BF_4]^-$, $[BMPY]^+$ $[Br]^-$ and $[EMPY]^+$ $[Br]^-$ using the PDP and EIS experimental data respectively

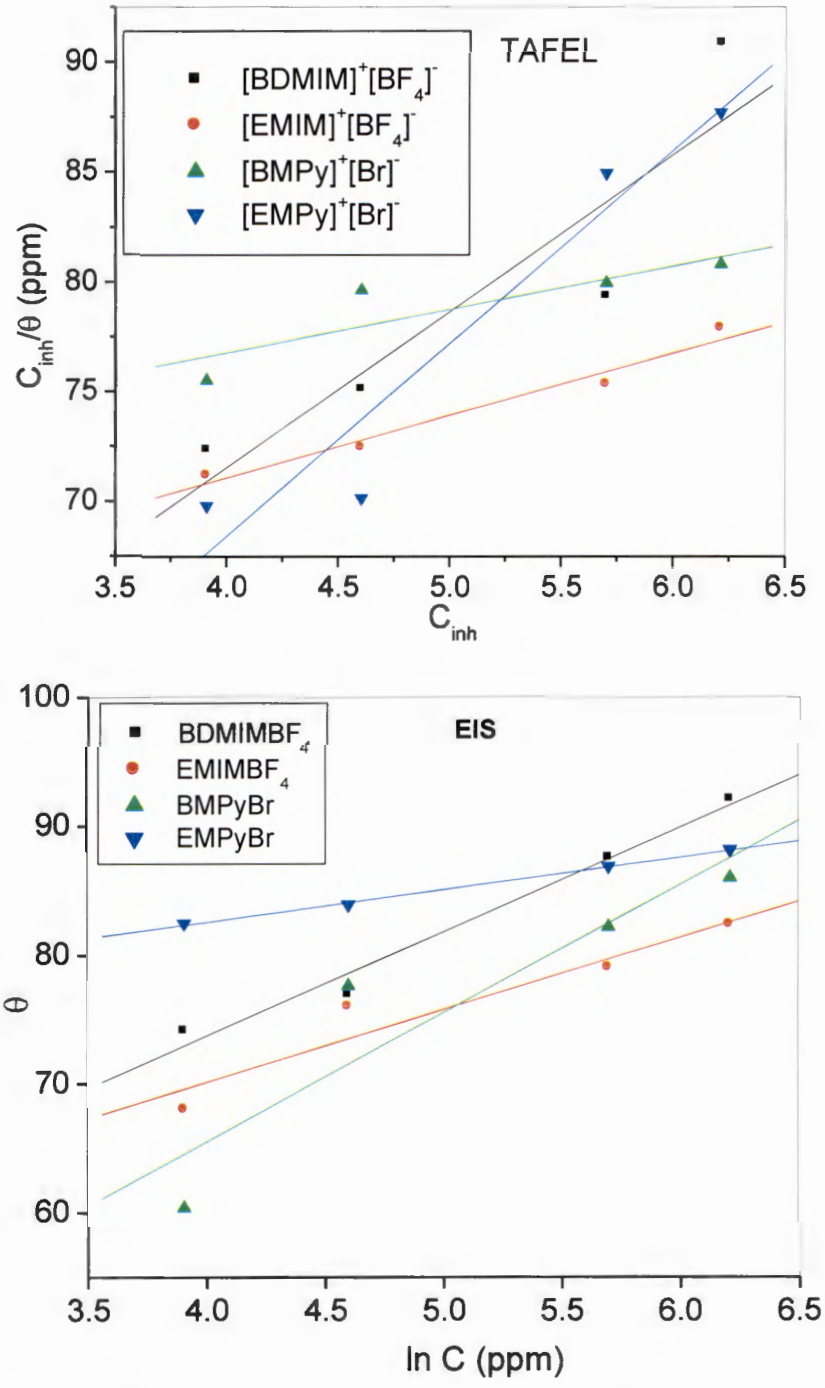

Figure 4.13: Temkin adsorption isotherm plot for $[BDMIM]^+$ $[BF_4]^-$, $[EMIM]^+$ $[BF_4]^-$, $[BMPY]^+[Br]^-$ and $[EMPY]^+$ $[Br]^-$ using the PDP and EIS experimental data respectively

Table 4.3: Adsorption parameters derived from the Langmuir and Temkin adsorption isotherm plots for the inhibitors.

Inhibitors	$-\Delta G^0_{ads}$ / kJ mol^{-1}		K_{ads} (x 10^3 mol^{-1})	
Langmuir adsorption isotherm				
	Tafel	EIS	Tafel	EIS
$[BDMIM]^+[BF_4]^-$	34.22 (0.9962)	32.84 (0.9996)	14.19	8.23
$[EMIM]^+[BF_4]^-$	33.70 (0.9998)	33.54 (0.9998)	11.54	10.84
$[BMPy]^+[Br]^-$	29.02 (1.0000)	33.20 (0.9997)	1.80	9.49
$[EMPy]^+[Br]^-$	32.72 (0.9996)	30.51 (1.0000)	7.84	3.26
Temkin Adsorption Isotherm				
	Tafel	EIS	Tafel	EIS
$[BDMIM]^+[BF_4]^-$	31.86 (0.9118)	31.97 (0.9900)	5.57	5.82
$[EMIM]^+[BF_4]^-$	30.55 (0.9835)	31.12 (0.9583)	3.31	4.16
$[BMPy]^+[Br]^-$	30.49 (0.8699)	32.99 (0.9227)	3.23	8.74
$[EMPy]^+[Br]^-$	31.97 (0.9624)	30.01 (1.0000)	5.82	2.67

( ) = R^2 values for the linear plots

4.3 FTIR SPECTROSCOPY

Fourier transform infrared spectroscopy was employed to study the ionic liquids interaction with mild steel surface. The FTIR spectra of pure ILs, and ILs with mild steel at an optimum concentration of inhibitor (500 ppm) at 303 K after 24 h immersion of mild steel specimens as shown in Figures 4.13-4.16. FTIR spectroscopy assisted in analysing the different regions of the electromagnetic spectrum. It also helped in structure and reactions of organic molecules and to understand how much energy corresponds to each wavelength and how this relates to the physical process after absorption of radiation. It is a powerful method for the identification of functional groups [118,119].

Important IR bands for $[BDMIM]^+[BF_4]^-$ were 2931 cm^{-1} , 2870 cm^{-1} , 2965 cm^{-1} ; and for pure $[EMIM]^+[BF_4]^-$were 1465 cm^{-1} and 2941 cm^{-1}, for $[BMPy]^+[Br]^-$ were 3467 cm^{-1}, 2962

cm^{-1}, 2873 cm^{-1}, 1615cm^{-1} and for $[EMPy]^+[Br]^-$ were 3451 cm^{-1}, 2970 cm^{-1}, 2288 cm^{-1} 2147 and 1738 cm^{-1}. The action of such inhibitors (imidazolium) depends on the specific interaction between the functional groups and the metal surface, due to the presence of the –C=N– group and electronegative nitrogen in the molecule.

It is later observed the prominent bands had disappeared upon the immersion of mild steel, due to the adsorption of inhibitor on the mild steel and new bands of $[BDMIM]^+[BF_4]^-$ and $[EMIM]^+[BF_4]^-$ that ranges between 3155 and 3318 cm^{-1} and for $[BMPy]^+[Br]^-$ and $[EMPy]^+[Br]^-$ its broad band is between 2901 cm^{-1} and 3100 cm^{-1}, had formed.

The band in $[BDMIM]^+[BF_4]^-$ at approximately 3500.cm^{-1} showed a massive change due to the formation of a new peak, having higher signal intensity. The changes in the infrared spectra of pure ILs confirms the changes in conformation of all ILs under study on the addition of an inhibitor.

Table 4.4 Characterization table of some major functional group with their Absorbance frequency Region.

Major functional group	Absorption frequency Region			
O-H	3650- 3590			
N-H	3500-3300	1650-1590	900-650	
=CH-H	3100-3070	1420-1410	900-880	
=C-H	3100-3000	2000-1600		
C-H	2900-2700	1440-1320		
=-CH_3	2880-2860	2970-2950	1380-1370	1470-1430
O-H	2700-2500	1320-1210	950-900	
$C \equiv C$	2140-2100			
C=O	1750-1700			
C=C	1600-1500			
C-N	1340-1250			
C-O-C	1200-1180			
-C-H	770-730			

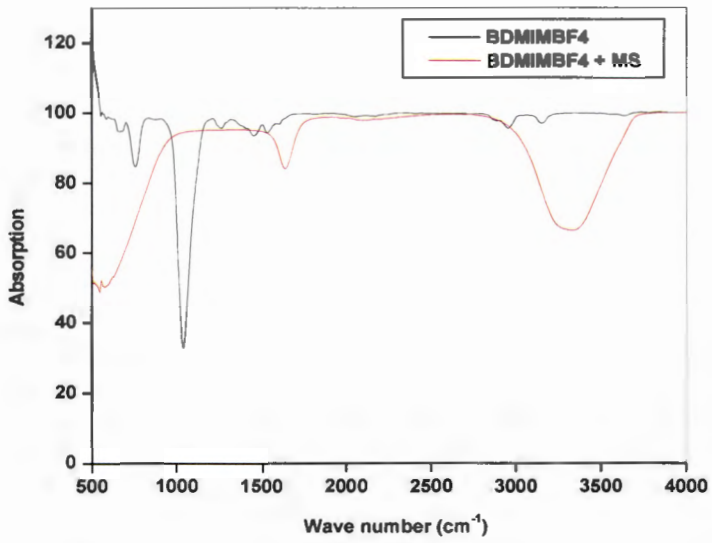

Figure 4.14: IR Spectra of pure $BDMIMBF_4$ and 500 ppm with Immersed MS

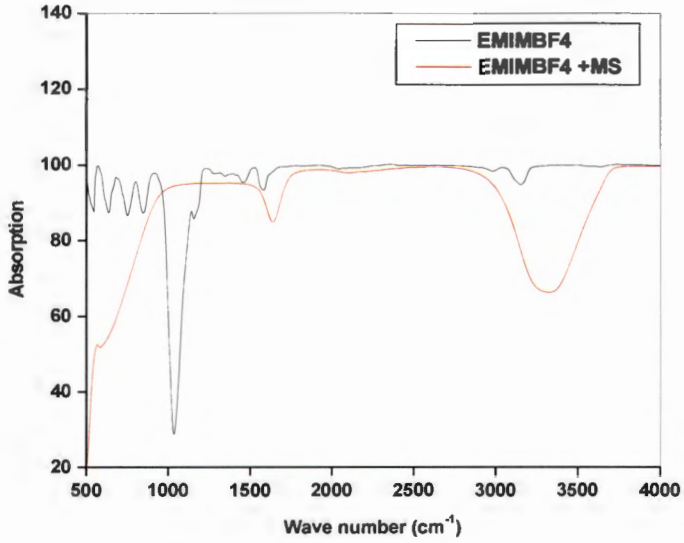

Figure 4.15: IR Spectra of pure $[EMIM]^+[BF_4]^-$ and 500 ppm with Immersed MS

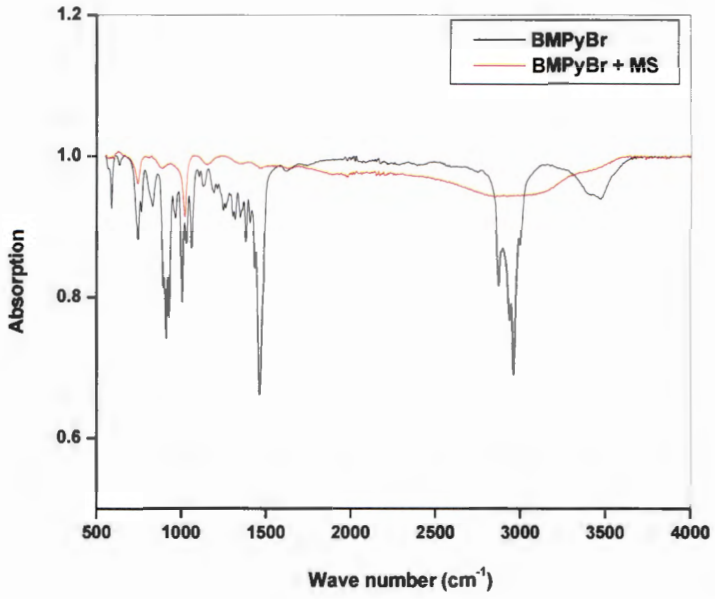

Figure 4.16: IR Spectra of pure $[BMPy]^+[Br]^-$ and 500 ppm with Immersed MS

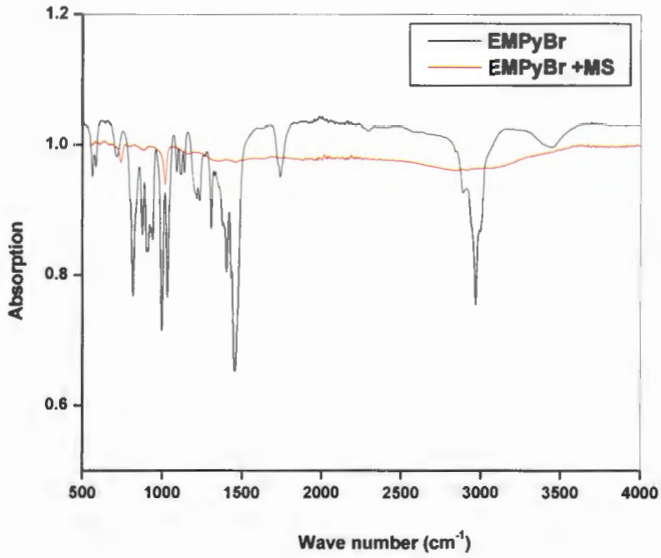

Figure 4.17: IR Spectra of pure $[EMPy]^+[Br]^-$ and 500 ppm with Immersed MS

4.4 ULTRAVIOLET-VISIBLE SPECTROPHOTOMETRY (UV)

UV-Visible spectroscopy is one of the fundamental principles of spectrophotometry that provides a strong evidence for the interaction of the metal with the ILs as inhibitor. As shown in figures 4.17 – 4.20, the UV-Visible absorption spectra of pure ILs, and ILs with mild steel at an optimum concentration of inhibitor (500 ppm) at 303 K after 24 h immersion of mild steel specimens. Before the mild steel immersion, the electronic absorption spectrum of both the inhibitors shows bands in the UV-Visible region due to π-π^* and n-π^* transitions with a considerable charge transfer character. After 24 h immersion of mild steel in the presence of inhibitors, the observed change in the position and absorbance of the absorption maximum indicate the interaction between the inhibitors and iron in solution. It is in These experimental findings that we obtain a strong evidence for the complex formed between Fe^{2+} and inhibitors in a 1 M HCl solution. UV-Visible observation confirms the formation of a protective film of metal-inhibitor complex on the metal surface. [120]

The similarity in values of λ_{max} and in the shape for the imidazolium ILs may be due to their common π-electrons nucleus (the imidazolium unit). The nucleus is the main substrate responsible for their UV-VIS absorption. This means that the alkyl chain length does not necessarily make a significant influence on the shape of the UV-VIS spectra for the imidazolium ILs. The broadening of the absorption peak after mild steel immersion is an evidence of the formation of IL/Fe complex The adsorption spectra of 500ppm ILs were recorded at different concentration at λ The adsorption spectra of the pure ILs show a single absorption peak at 228nm, 223nm, 219nm, 221nm for, $[BDMIM]^+[BF_4]^-$ $[EMIM]^+[BF_4]^-$, $[BMPy]^+[Br]^-$, and $[EMPy]^+[Br]^-$ respectively corresponding to π-π^* and/ or n-π^* transitions. There was an additional peak for the UV- vis spectrum of all ILs under study. Upon mild steel immersion, there is a significant change in the UV- vis absorption spectra of the inhibitors appearing at 215nm, 215nm, for $BDMIMBF_4$ and $EMIMBF_4$, respectively, whereas the characterization of pure BMPyBr, and EMPyBr are not clear. This is sometimes caused by impurities or high concentration of pure BMPyBr, and EMPyBr The pure ILs however of $BDMIMBF_4$, and $EMIMBF_4$, show a slightly blue shift for both which later, its spectra further had a blue shift. This blue shift in the wavelength of the maximum absorbance is attributed to

the formation of Fe/IL complex. New peaks can be seen on $BDMIMBF_4$, and $EMIMBF_4$. The new peak can be attributed to the transition between π-bonding of the Fe/IL complex and the π^* orbital of the anion. [121]

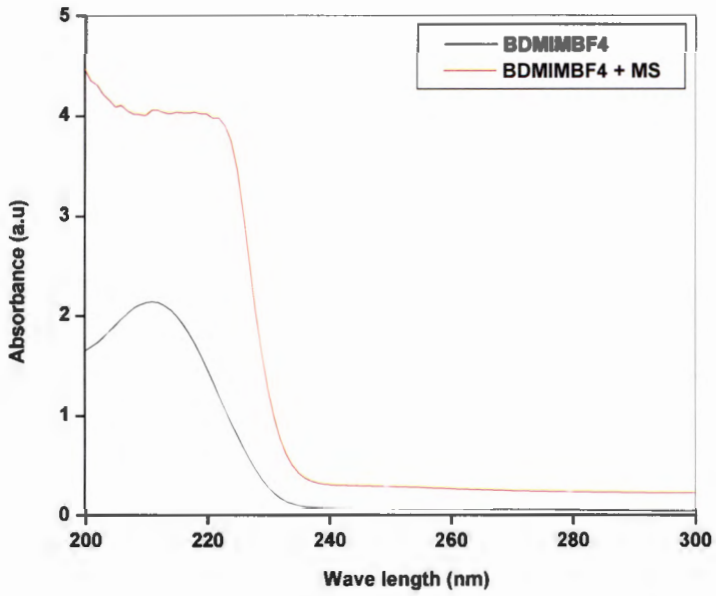

Figure 4.18: UV-Vis Spectra of pure $[BDMIM]^+[BF_4]^-$ and 500 ppm with Immersed MS

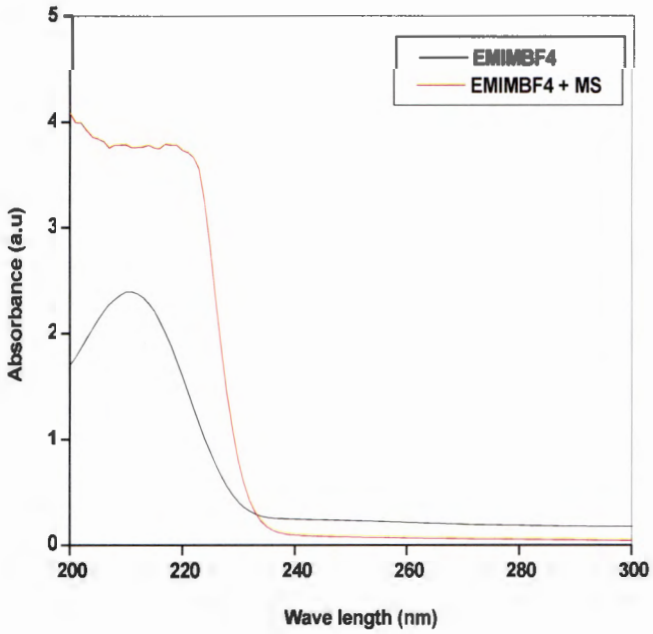

Figure 4.19: UV-Vis Spectra of pure $[EMIM]^+[BF_4]^-$ and 500 ppm with Immersed MS

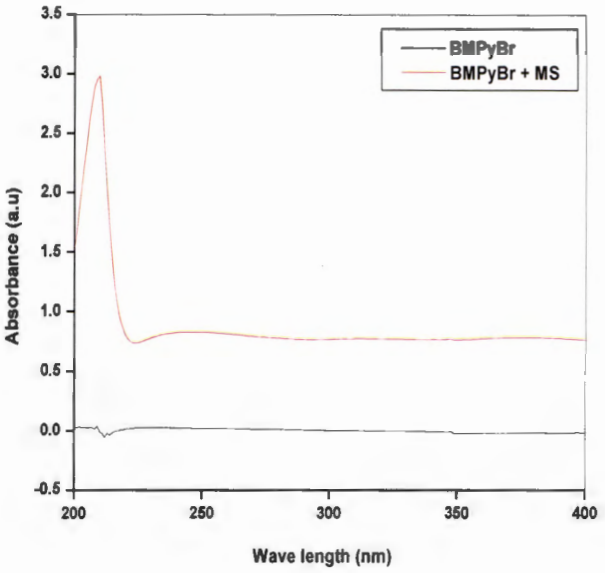

Figure 4.20: UV-Vis Spectra of pure $[BMPy]^{+}[Br]^{-}$ and 500 ppm with Immersed MS

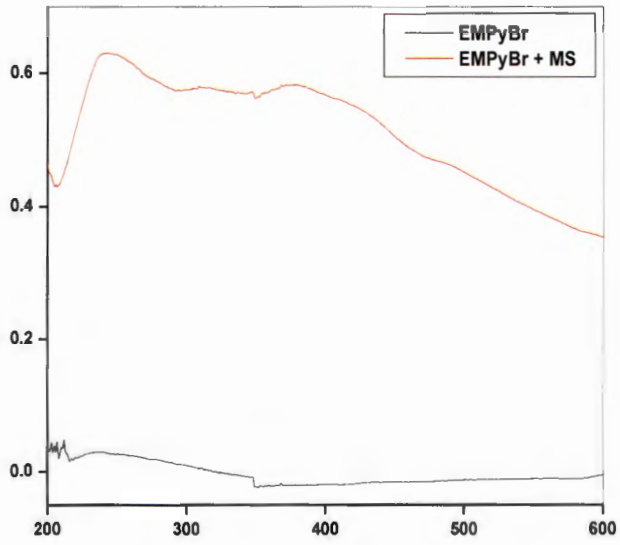

Figure 4.21: UV-Vis Spectra of pure $[EMPy]^{+}[Br]^{-}$ and 500 ppm with Immersed MS

4.5 Raman Spectroscopy

Raman spectroscopy, a molecular spectroscopy which is observed as inelastically scattered light, allows for the interrogation and identification of vibrational (phonon) states of molecules. It provides an invaluable analytical tool for molecular finger printing as well as monitoring changes in molecular bond structure, which includes, state changes, stresses & strains. This type of spectroscopy has advantages over other type of spectroscopic methods such as FTIR and the NIR. These advantages stem from the fact that the Raman effect manifests itself in the light scattered off of a sample as opposed to the light absorbed by a sample. As a result, Raman spectroscopy requires little to no sample preparation and is insensitive to aqueous absorption bands. This property of Raman facilitates the measurement of solids, liquids, and gases not only directly, but also through transparent containers such as glass, quartz, and plastic. A Raman spectral library enables us to see how easily Raman spectra can be used for material identification and verification. One of the two ways, the classical wave interpretation or the quantum particle interpretation, is expected when performing the Raman scattering analysis [122].

Raman spectroscopy of the molecules under study was classified on the ability to measure a shift in wavelength or the frequency. It is imperative that a monochromatic excitation source be employed. While a laser is typically the best excitation source, not all lasers are suitable for Raman spectroscopy, so it is essential that the laser frequency is extremely stable and does not mode hop, since this will cause errors in the Raman shift. A clean, narrow bandwidth laser was used in this analysis , this is because, the quality of the Raman peaks is directly affected by the sharpness and stability of the excitation light source, the shorter the wavelength, the more powerful the Raman signal, however, this is not the only consideration especially when dealing with organic molecules. The Raman spectra of pure ILs, and ILs with mild steel at an optimum concentration of inhibitor (500 ppm) at 303 K after 24 h immersion of mild steel specimens as shown in Figures 4.21 – 4.24.

The effective Raman scattering of iron corrosion products allows their detection even with excitations at low Laser power with reasonable spectra accumulation time, and their respective spectra exhibit characteristics features which clearly fingerprint their structural nature and state. The Raman spectral shapes could be strongly affected by excitation wavelength (resonance effect) and spectrometric specifications therefore their setup was carried out with precautions. The recorded Raman spectra Figures 4.22- 4.25, displayed Raman scattering of ILs BMPyBr, EMPyBr and $BDMIMBF_4$ which are presented by spectrum characterized at 1250 cm^{-1} 1345 cm^{-1}.and 1560 cm^{-1} band respectively. Whereas $EMIMBF_4$ present weaker spectra with fewer vibrational bands with minimal specification of their phases, probably due to difficulty in their detection or distinction structural characterization.

The Raman spectrum of EMPyBr is similar to that of BMPyBr which shows a shifting in the spectrum. The Raman bands observed at 758 and 793 cm^{-1} corresponds to C-H vibration. The bands at 1474 and 1540 cm^{-1} correspond to C=C stretching vibrations and the one at 1658 cm^{-1} corresponds to asymmetric stretching of $N\text{-}CH_2$ or $CN\text{-}CH_3$ stretching vibration. The main bands at 2918 and 2959 cm^{-1} corresponds to asymmetric mode of CH_2 stretching vibration. $BDMIMBF_4$ has intensive bands at 3056 cm^{-1} to 3105 cm^{-1} that corresponds to symmetric stretching vibration of CH_3 and CH_2 . The characteristic Raman bands observed in pure ILs have disappeared after mild steel immersion. This is an indication of IL/Fe complex formation.[123]

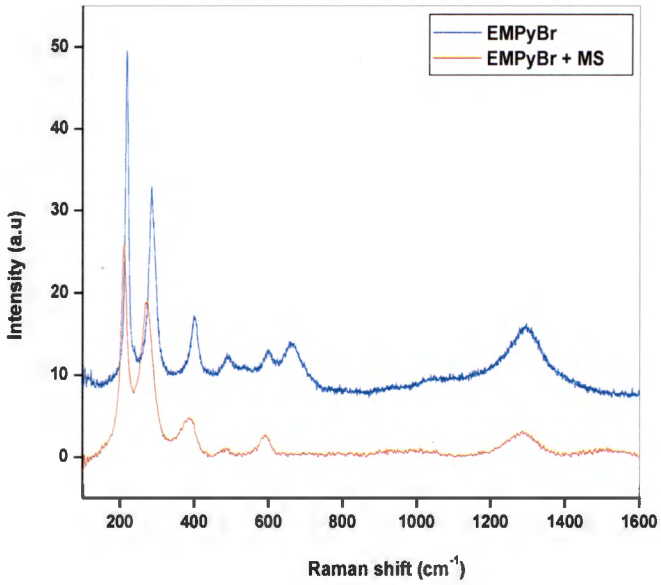

Figure 4.22: Raman Spectra of pure $[EMPy]^{+}[Br]^{-}$ and 500 ppm with Immersed MS

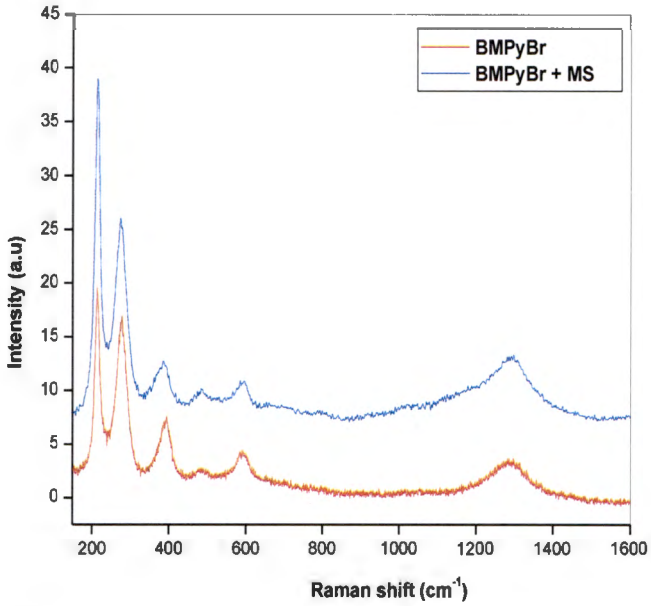

Figure 4.23: Raman Spectra of pure $[BMPy]^{+}[Br]^{-}$ and 500 ppm with Immersed MS

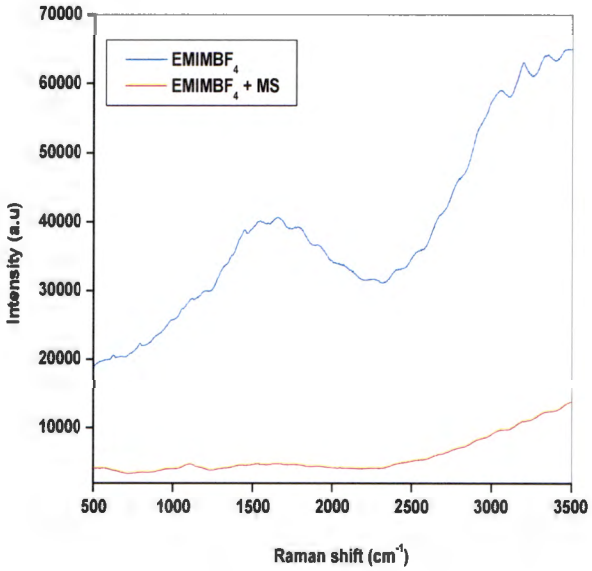

Figure 4.24: Raman Spectra of pure $[EMIM]^+[BF_4]^-$ and 500 ppm with Immersed MS

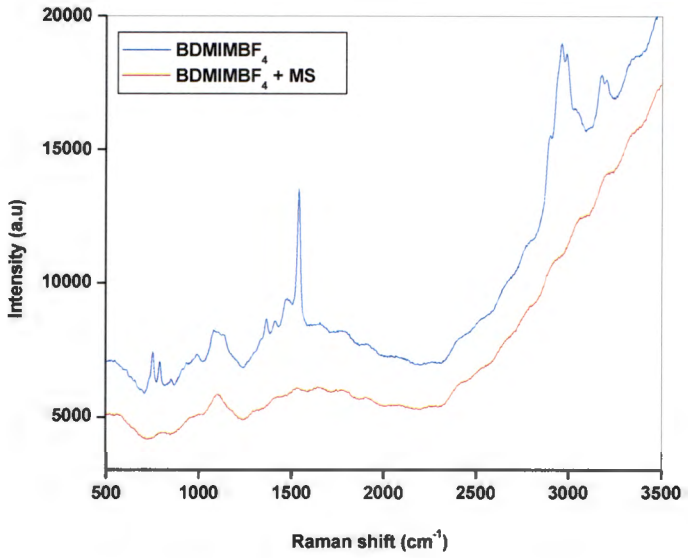

Figure 4.25: Raman Spectra of pure $[BDMIM]^+[BF_4]^-$ and 500 ppm with Immersed MS

4.6. Quantum Chemical Calculations

4.6.1 Optimised structures, HOMO and LUMO densities for the studied ionic liquids

The inhibition efficiency observed from several experimental methods have been supported by DFT based quantum chemical calculations. Several DFT based parameters such as energies of frontier molecular orbitals (E_{HOMO}, E_{LUMO}), energy band gap (ΔE), electronegativity (χ), hardness (η), softness (σ), dipole moment (μ) etc. were computed through which the adsorption behaviour of these compounds have been described over the metallic surface. A good correlation between experimental and DFT study have been derived. The optimised structures as well as the highest occupied molecular orbital (HOMO) and lowest unoccupied molecular orbital (LUMO) densities are shown in Figure 4.26. In [BDMIM][BF_4]and [EMIM][BF_4], the HOMO density is delocalized throughout the cation and anion of the ionic liquid while in [BMPy][Br] and [EMPy][Br], the HOMO is entirely on the anion part of the ionic liquid. This information implies that for the former structures, both the anion and the cation can be considered as sites of high electron density while for the latter structures the site of high electron density is the anion. In this way, when BMPyBr and EMPyBr interact with the metal surface, it is expected that the anion will donate electrons to the metal surface. The LUMO density is entirely on the cation part of the ionic liquids in all the compounds studied. This implies that in the case of back-donation mechanism from the metal to the inhibitor, electrons donated by the metal ions are likely to be transferred to the cation part of the inhibitor molecule. [124]

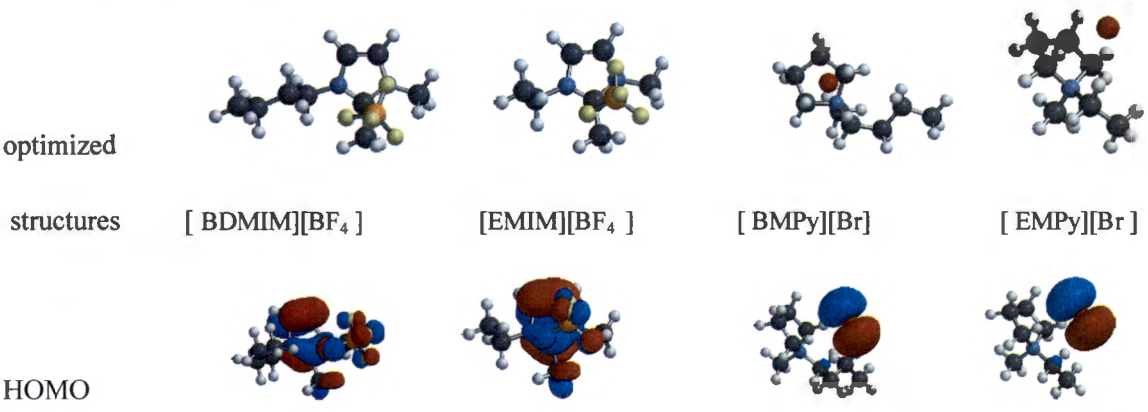

LUMO

Density

Figure 4.26. Optimized conformers, HOMO density and LUMO density for the studied ionic liquids

4.6.2. Quantum chemical parameters

Table 4.5 reports the quantum chemical parameters investigated in this work. Previous studies have shown that quantum chemical parameters such as the energy of the HOMO (E_{HOMO}), energy of the LUMO (E_{LUMO}), energy band gap (ΔE), dipole moment, etc., can be utilised to understand the adsorption phenomenon of the inhibitor on the metal surface. However, it is important to mention here that the information about the molecular reactivity obtained from these quantum chemical descriptors cannot directly be interpreted into corrosion inhibition efficiency, because the adsorbability of an effective corrosion inhibitor involves more processes such as film formation and the nature of the metal surface. It is for this reason that in some cases a comparison between calculated quantum chemical parameters and inhibition efficiency does not yield a good correlation [125].

The energy of the HOMO (E_{HOMO}) is related to the ability of the molecule to donate electrons, while the energy of the LUMO (E_{LUMO}) is related to the ability of the molecule to accept electrons. The higher the value of E_{HOMO}, the greater is the ability of the molecule to donate electrons, and the lower the value of E_{LUMO}, the stronger is the tendency of the molecule to accept electrons. The energy difference (ΔE) also informs about the reactivity of the studied molecules. Molecules with a small ΔE value have a greater reactivity than molecules that have a large ΔE value [126]. The results for the studied ionic liquids (reported in Table 4.5) show that the tendency to donate electrons to the partially filled d orbital of the metal follows the $[EMPy]^+[Br]^-$ > $[BMPy]^+[Br]^-$ > $[BDMIM]^+$ $[BF_4]^-$ > $[EMIM]^+[$ $BF_4]^-$. The trend identified here is significantly different from the trend in the inhibition efficiency

(section 4.1), where it is reported that the highest inhibition efficiency is that of $[BDMIM]^+$ $[BF_4]^-$. The tendency to accept electrons follow the order $[EMIM]^+[BF_4]^- < [BDMIM]^+$ $[BF_4]^- < [BMPy]^+[Br]^- < [EMPy]^+[Br]^-$. The trend in the E_{LUMO} is also significantly different from the trend obtained in the inhibition efficiency. The trend in the energy gap (ΔE) also suggest that the order of the reactivity among the species should be $[BMPy]^+[Br]^- >$ $[EMPy]^+[Br]^- > [BDMIM]^+$ $[BF_4]^- > [EMIM]^+[BF_4]^-$. This trend is also significantly different from the experimental findings. The preference for the $[BMPy]^+[Br]^-$ and $[EMPy]^+[Br]^-$ ionic liquids may be related to the fact that the HOMO is entirely localised on the bromide anion, which can easily donate electrons because it has lower electronegativity than fluoride ion.

Table 4.5 Quantum chemical parameters for the studied ionic liquids

Quantum chemical parameters	**$[EMIM]^+[BF_4]^-$**	**$[BDMIM]^+$ $[BF_4]^-$**	**$[EMPy]^+[Br]^-$**	**$[BMPy]^+[Br]^-$**
E_{HOMO}	-7.44	-7.350	-4.610	-4.620
E_{LUMO}	-0.73	-0.650	0.680	0.660
ΔE	6.71	6.700	5.290	5.280
Hardness	3.355	3.350	2.645	2.640
Softness	0.298	0.299	0.378	0.379
Electron affinity	0.73	0.650	-0.680	-0.66
Ionisation potential	7.44	7.350	4.610	4.62
Dipole moment	11.41	11.29	12.97	12.66
Electronegativity	4.085	4.000	1.965	1.980
Global electrophilicity	2.487	2.388	0.730	0.743
%IE	77.93	90.84	87.70	80.82

Global hardness (η) and softness (σ) are molecular properties that also facilitate the analysis of molecular reactivity and selectivity. These quantities are often associated with the Lewis theory of acids and bases and Pearson's hard and soft acids and bases; a hard molecule has a large ΔE and therefore is less reactive; a soft molecule has a small ΔE and is therefore more reactive.[127] Adsorption occurs most probably at the region of the molecule where σ has the highest value. The values of σ reported in Table 4.5 show that the adsorbability follows the order $[BMPy]^+[Br]^-$ > $[EMPy]^+[Br]^-$ > $[BDMIM]^+$ $[BF_4]^-$ > $[EMIM]^+[$ $BF_4]^-$. The results reported here agree well with the results reported on the energy of the HOMO. The dipole moment is another indicator of the electronic distribution in molecules, and it is a good indicator of the hydrophilic/hydrophobic character of a given system. A high dipole moment indicates polar character for the molecule, while a low dipole moment indicates nonpolar character for the molecule. Trends in the calculated dipole moments and observed inhibition efficiency are not always univocal [128, 125]

The results in the present study show that the dipole moment increases following the order $[EMPy]^+[Br]^-$ > $[BMPy]^+[Br]^-$ > $[EMIM]^+[$ $BF_4]^-$ > $[BDMIM]^+$ $[BF_4]^-$.

The adsorbability of an inhibitor on the metal surface is also related to the charges on the chelating atom. The higher the negative partial atomic charge of the adsorbed centre, the more easily the atom donates its electron to the partially filled or vacant *d* orbital of the metal. The Mulliken atomic charges on the atoms of the studied molecules are reported in Figure 4.27. The highest negative charge is on the Br^- ion, indicating that it has the highest tendency to donate electron. This means that, from theoretical calculations, ionic liquids with bromide ions should be better corrosion inhibitors than ionic liquids with the tetrafluoroborate anion, which agrees well with the studies on the HOMO-LUMO energies and global softness parameters [128].

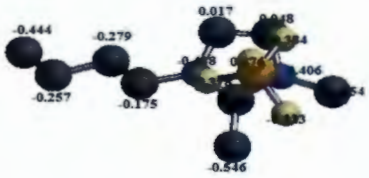

$[BDMIM]^+ [BF_4]^-$

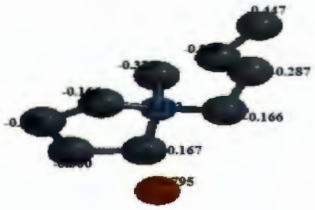

$[BMPy]^+[Br]^-$

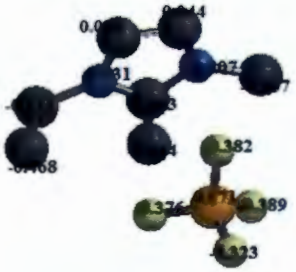

$[EMIM]^+[BF_4]^-$

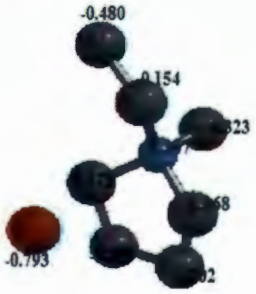

$[EMPy]^+[Br]^-$

Figure.4.27 Partial Mullikan atomic charges on the atoms of the studied ionic liquids.

The local selectivity of an inhibitor (i.e., the site on the molecule at which a particular reaction is likely to occur) is often analysed by using condensed Fukui functions. These functions (indices) provide information about which atoms in a molecule have a higher tendency to either donate or accept an electron or pair of electrons [129,130]. The nucleophilic and electrophilic Fukui functions can be calculated using the finite difference approximation, as shown in equation 32 and 33.

The preferred site for nucleophilic attack is the atom or region in the molecule where the value of f^+ is the highest, while the preferred site for electrophilic attack is the atom or region in the molecule where the value of f^- is the highest. The calculated values of the Fukui functions for the non-hydrogen atoms in the four ionic liquids are reported in Table 4.6. The value of f^+ is highest on C6, in both $[EMPy]^+[Br]^-$ and $[BMPy]^+[Br]^-$, which indicates that the cation is an easy electron poor centre. The value of f^+ is highest on C1 in $[BDMIM]^+$

$[BF_4]^-$ and both C1 and C8 in $[EMIM]^+[BF_4]^-$, which again indicates that the preferred site for nucleophilic attack is on the cation part of the ionic liquids.

The value of f^- is highest on Br^- ion (with a value of -0.820) for both $[EMPy]^+[Br]^-$ and $[BMPy]^+[Br]^-$, which suggests that in these two ionic liquids, the preferred site for interaction with the metal surface is the Br^- ion on the inhibitor molecule. The value of f^- is highest on F3 for both $[EMIM]^+[BF_4]^-$ and $[BDMIM]^+[BF_4]^-$ ionic liquids, indicating that the preferred site for interaction between the inhibitor and the metal surface is the fluoride ion. When The f^- value is compared between the results on $[EMPy]^+[Br]^-$ and $[BMPy]^+[Br]^-$ and the result on $[EMIM]^+[BF_4]^-$ and $[BDMIM]^+[BF_4]^-$ ionic liquids shows that f^- value is highest for $[EMPy]^+[Br]^-$ and $[BMPy]^+[Br]^-$, which suggests that the Br^- ion is a better site to interact with the metal surface than F^-, which agrees well with the previous findings on quantum chemical parameters reported in this work. However due to the π and –C=N- bonds found in the imidazolium cycle, discussed earlier, the imidazolium compound $[BDMIM]^+[BF_4]^-$ exhibited a higher inhibition efficiency as compared to Pyrollidinium ILs.[103, 105, 107].

Table 4.6 (a-d) . Fukui functions on the atoms of the four ionic liquid

4.6 a) Fukui functions on $[BMPy]^+[Br]^-$ ionic liquid

Atom number	Charge on neutral	Charge on cation	Charge on anion	f^+	f^-
N1	-0.373	-0.374	-0.344	0.029	0.001
C2	-0.166	-0.167	-0.131	0.035	0.001
C3	-0.302	-0.311	-0.239	0.063	0.009
C4	-0.300	-0.313	-0.245	0.055	0.013
C5	-0.167	-0.172	-0.122	0.045	0.005
C6	-0.322	-0.344	-0.218	0.104	0.022
C7	-0.166	-0.165	-0.127	0.039	-0.001
C8	-0.287	-0.294	-0.225	0.062	0.007
C9	-0.266	-0.272	-0.229	0.037	0.006
C10	-0.447	-0.451	-0.437	0.010	0.004
Br	-0.795	0.025	-0.860	-0.065	-0.820

4.6 b) Fukui functions on $[EMPy]^+[Br]^-$ ionic liquid

Atom number	Charge on neutral	Charge on cation	Charge on anion	f^+	f^-
N1	-0.367	-0.368	-0.335	0.032	0.001
C2	-0.168	-0.178	-0.119	0.049	0.010
C3	-0.302	-0.311	-0.238	0.064	0.009
C4	-0.299	-0.313	-0.234	0.065	0.014
C5	-0.171	-0.166	-0.133	0.038	-0.005
C6	-0.323	-0.345	-0.216	0.107	0.022
C7	-0.145	-0.155	-0.105	0.040	0.010
C8	-0.480	-0.485	-0.418	0.062	0.005
Br	-0.793	0.028	-0.863	-0.070	-0.821

4.6 c) Fukui functions on $[BDMIM]^+$ $[BF_4]^-$ ionic liquid

Atom number	Charge on neutral	Charge on cation	Charge on anion	f^+	f^-
C1	0.603	0.639	0.456	-0.147	-0.036
N2	-0.406	-0.406	-0.423	-0.017	0.000
C3	0.048	0.118	0.025	-0.023	-0.070
C4	0.017	0.097	-0.029	-0.046	-0.08
N5	-0.438	-0.433	-0.456	-0.018	-0.005
C6	-0.175	-0.204	-0.133	0.042	0.029
C7	-0.279	-0.291	-0.257	0.022	0.012
C8	-0.257	-0.267	-0.254	0.003	0.010
C9	-0.444	-0.450	-0.436	0.008	0.006
C10	-0.546	-0.549	-0.529	0.017	0.003
C11	-0.354	-0.374	-0.318	0.036	0.020
F1	-0.384	-0.349	-0.382	0.002	-0.035
F2	-0.378	-0.311	-0.371	0.007	-0.067
F3	-0.323	-0.218	-0.345	-0.022	-0.105
F4	-0.376	-0.326	-0.382	-0.006	-0.050
B	0.664	0.700	0.655	-0.009	-0.036

4.6 d) Fukui functions on $[EMIM]^+[BF_4]^-$ ionic liquid

Atom number	Charge on neutral	Charge on cation	Charge on anion	f^+	f^-
C1	0.603	0.641	0.459	-0.144	-0.038
N2	-0.407	-0.402	-0.423	-0.016	-0.005
C3	0.044	0.112	0.019	-0.025	-0.068
C4	0.023	0.107	-0.022	-0.045	-0.084
N5	-0.431	-0.430	-0.450	-0.019	-0.001
C6	-0.171	-0.203	-0.124	0.047	0.032
C7	-0.468	-0.478	-0.445	0.023	0.010
C8	0.357	-0.375	-0.322	-0.679	0.732
C9	-0.544	-0.547	-0.524	0.020	0.003
F1	-0.389	-0.345	-0.383	0.006	-0.044
F2	-0.382	-0.332	-0.383	-0.001	-0.050
F3	-0.323	-0.217	-0.345	-0.022	-0.106
F4	-0.376	-0.306	-0.378	-0.002	-0.070
B	0.671	0.709	0.663	-0.008	-0.038

RECOMMENDATION

The electrochemical and DFT analyses suggests that all tested ionic liquids act as good inhibitors towards mild steel corrosion in acidic solution of 1M HCl. Results showed the $[BDMIM]^+[BF_4]^-$, $[EMIM]^+[BF_4]^-$, $[BMPy]^+[Br]^-$ and $[EMPy]^+[Br]^-$ gave the inhibition performances of 90.84%, 77.93%, 80.82% and 87.70% respectively, at 500 ppm concentration attesting to the fact that these ionic liquids are suitable and relevant for industrial usage for further improvement on metal protection. Owing to their high inhibition efficiency, these ionic liquids shall be further tested for inhibition of other metallic corrosion in acidic and other corrosive environments.

SUMMARY AND CONCLUSIONS

Corrosion inhibition properties of imidazolium and pyrollidinium ILs, namely 1-ethyl-3-methylimidazolium tetrafluoroborate $[EMIM]^+[BF_4]^-$, 1-butyl-2,3-dimethylimidazoliumtetrafluoroborate $[BDMIM]^+[BF_4]^-$, 1-butyl-1-methylpyrrolidinium bromide $[BMPy]^+[Br]^-$ and 1-ethyl-1-methylpyrrolidinium bromide[$BMPy]^+[Br]^-$ were investigated on mild steel in 1 M HCl using electrochemical methods, spectroscopic techniques are quantum chemical calculations. The following conclusions were drawn from the results:

a) The four ILs studied in this work showed appreciable inhibition efficiencies for mild steel corrosion in 1 M HCl and the inhibition efficiency increased with increasing concentration of the inhibitors.
b) Potentiodynamic polarization study showed that the studied ILs are mixed type inhibitors and the EIS study revealed that the ILs form protective film on mild steel surface.
c) The experimental results showed that the studied ILs adsorb spontaneously on mild steel surface and the data fits to the Langmuir adsorption isotherm. The adsorption process involves both physisorption and chemisorption mechanisms.
d) FTIR, UV-vis and Raman spectra revealed the occurrence of chemical interactions between the ILs and iron in the mild steel.
e) Quantum chemical parameters such as the E_{HOMO}, chemical hardness and dipole moment agree with experimental results.

f) Both experimental and quantum chemical results showed that the inhibition efficiency of ILs is affected by the length of the alkyl side chain, and the order of inhibition efficiency for the studied compounds is; $[BDMIM]^+[BF_4]^-$ > $[EMPy]^+[Br]^-$ > $[BMPy]^+[Br]^-$ > $[EMIM]^+[BF_4]^-$.

REFERENCES

1. F. Raspall. Design with material Uncertainty Response Design and Fabrication in Architecture, Model. Behav., 1(2015) 315-319.
2. L. C. Murulana, A. K. Singh, S. K. Skukla, M.M. Kabanda, E.E. Ebenso, Experimental and quantum chemical studies of some Bis (triflouromethyl-sulfonyl) Imide Imidazolium-Based Ionic Liquids as corrosion Inhibitors for Mild Steel in Hydrochloric Acid Solution, Ind. End. Res. 51 (2012) 13282-13299.
3. D. Chandran, H. Kiat-Ng, H. L. Nang -Lan, S. Gan, Investigation of the effects of palm biodiesel dissolved Oxygen and Conductivity on metal corrosion and elastomen degradation under novel Immersion method, Applied Therm. Eng., 104 (2016) 294-308.
4. Z. Ahmad, Principles of corrosion Engineering and Corrosion Control. J. Corros. Sci., 1 (2006) 1-8.
5. M. Stratmann, K. Bohnenkamp, H. J. Enegell, An Electrochemical study of phase-transition in rust layers. Corros. Sci., 23 (1983) 969-985.
6. J. O. Nriagu, A global assessment of natural source of atmospheric trace metal. Atmos. res., 338 (1989) 47-49.
7. G. H. Kock, M. P. H. Brongers, N. G. Thompson, Corrosion costs and preventative strategies in the United States. J. Corros. Sci., 1 (2002) 1-12.
8. R. A. Gummow, Examining the controversy surrounding the -850mVCP criteria Pipeline Gas .J. Atmosph.Sol-Terrest. Phy., 237 (2010) 85-87.
9. M. Dudukcu, Electrochemical Synthesis and Corrosion Inhibition of poly-5-aminoindole on Stainless Steel. J. Corros. Sci., 97 (2016) 110-114.
10. C. Zhang, Z. Zhang, L. Lin, Degradation in pitting resistance of 316L Stainless Steel under hydrostatic pressure. Electrochimia. Acta., 210(2016) 989.
11. S. S. Abd El-Rehim, M. A. M. Ibrahim, K. F. Khaled, 4 Aminoantipyrine as an inhibitor of mild steel corrosion in HCl solution, J. Appl. Electrochem., 29(1999) 593-599.
12. B. N. Popor. Pitting and Crevice Corrosion. Corros. Eng., 7(2015) 289-325

13. H. P. Seifert, S. Ritter, J. Hickling, Researches and Service experience with environmentally assisted cracking of low-alloy Steel pressure-boundary Components under LWR conditions. Power Plant Chem., 6(2004) 111-113
14. R. M. Fernandez-Domene, E. Blasco-Tamarit, D. M. Gracia-Anton, Cavitation Corrosion repassivation kinetics of Titanium in heavy brine LiBr solution evaluated by using electrochemical techniques and confocal laser scanning microscopy. Electrochimica. Acta., 58(2011) 264-275.
15. E. E. Ebenso, Effect of halide ions on the corrosion inhibition of mild steel in H_2SO_4 using methyl red, Part 1, Bull. Electrochem. 19 (2003) 209-216.
16. S. S. Rajahram, T. J. Harvey, R. J. K. Wood, Electrochemical investigation of erosion-corrosion using a slurry pot erosion tester, Tribolog. Int., 44(3),(2011) 232-240
17. R. J. K. Wood, A. J. Speyer, K. S. Tan. Investigation of erosion-corrosion processes using electrochemical noise measurement, Tribolog. Int., 35(2002) 613-614.
18. B. Tristchler, B. Forest, J. Rieu. Fretting Corrosion of materials for orthopaedic implants: a study of a metal/polymer contact in an artificial physiological medium, Tribilog. Int., 32(1999) 587-596.
19. K. A. Litchi, M. Ko, L. Wallis. Galvanic corrosion study of carbon steel to arsenic and antimony couples. Geothermic., 58(2015) 15-21.
20. Y. Tan, S. Bailey, B. Kinsella. Mapping non-uniform corrosion using the wire beam electrode method 3. Water-line corrosion. Corros. Sci., 43(2001) 1931-1937
21. M. R. Maheri, A. Abdollahi, The effects of long term Uniform Corrosion on the buckling of the ground based steel tanks under seismic loading. Corros. Sci., 154(2015) 1-9.
22. Y. Zhou, Y. Zou. The intergranular corrosion of mild steel in CO_2 + $NaNO_2$ solution. Electrochimia. Acta., 154 (2013) 157-165.
23. S. Li, Y. He, S.Hu, P. Zhang. Evaluation of the steel of grain size on chromium carbide precipitation and intergranular corrosion of 316L Stainless Steel. Corros. Sci., 68(2013) 249-255.
24. H. Wall, L. Wadiso, Corrosion measurement in steel sheet pile walls in a marine environment. Marine structure. 33(2013) 21-32.

25. S. Rhode, V. Kain, V.S. Raja, G. J. Abraham, Factors affecting Corrosion behaviour of inclusion containing stainless steels: a scanning electrochemical microscopic study, Mater. Charact., 77(2013) 109-115.
26. N. Hackerman, Effect of temperature on corrosion of metals by water, Ind. Eng. Chem., 44(1952) 1752-1755.
27. H. H. Uglig, J. Wiley, Corrosion and corrosion control., 1(1963) 329.
28. A. Chandhari, N. Nitin, Role of Oxygen Scavengers in limiting oxygen permeation into emulsions and improving stability of encapsuled retinol. J. Food Eng., 157 (2015) 7-13.
29. R. Baboian, G. Haynes, R. Turcotte, Galvanic Corrosion on Automobiles, Galvanic Corrosion. ASTMSTP978, Am. Soc. Test. Mater., (1988) 249-259.
30. V. Brusic, M. Russak, R. Schad, G. Frankel, A Selius, D. Dimilia, D. Edmonson. Corrosion of thin film magnetic disc: Galvanic effects of the carbon overcoat. J. Electrochem. Soc., 136 (198) 235-249
31. R. Baboian, G. Haynes, Galvanic Corrosion of fertile stainless steel in seawater. Corrosion in natural Environments, ASTM STP 558, W.H. Ailor, S.W. Dean, F.H. Haynie(Eds), Am. Soc. Test. Mater., (1974) 171-184.
32. J.D. Yoo, K. Ogle, P. Volovitch, The effect of synthesis zinc corrosion products on corrosion of electrogalvanized steel in presence of zinc Corrosion products. Corros. Sci., 83 (2014) 32-37.
33. N.J. Bunce, L. Lui, J. Zhu, D. Alane, Reaction of naphthalene and its derivatives with hydroxyl radicals in the gas phase. Environ. Sci., 31(1997) 2252-2259.
34. B. Puga, S. Joivet, V. Vivier, V. Charbonnier, H. Guerron, J. Zhang, Electrochemical properties and dissolution mechanism of A_2 Ni_7 hydrides (A=Y,Gd, La-Sm), Electrochem., 2(2015) 1321-1330.
35. R.E. Wilson, The mechanism of the corrosion of iron and steel in natural waters and the calculation of specific rates of corrosion. Ind. Eng. Chem., 15 (1923) 127-133
36. R.M. Burns. The corrosion of metals-1, Mech. Corros. Proc., 15 (1936) 20-38.
37. L. Joska, M. Marek, J. Leither, The mechanism of corrosion of palladium-silver binary alloys in artificial saliva. Corros. Sci., 14(2005) 1605-1611.

38. M. Noori, K. Jafarzadeh, A. Kashi, A study on corrosion and deactivation mechanism of Pt/Nb anodes in sodium chlorate containing solution using EIS, J. Electroanalytical chem., 772(2015) 27-37.
39. A. Tozar, I.H. Karahan, Structural and corrosion protection properties of electrochemically deposited nano-sized Zn-Ni alloy coatings. Appl. Surf. Sci., 318(2014) 15-23.
40. B. Elsener, U. Augst, Corrosion inhibitors for reinforced concrete., Sci. Tech. concrete Admixtures., 1(2016) 321-339.
41. F. Deflorian, S Rossi, M. Fedel, L.G. Ecco, R. Paganica, M. Bastorol. Study of the effect of corrosion inhibitors on power coatings applied steel. Prog. Org. Coat.,77 (2014) 2133-2139
42. K.R. Ausari, M.A. Quraishi, BisSchiff bases of isatin as new environmentally benign corrosion inhibitor for mild steel, J. Ind. Eng. Chem.,20 (2014) 2819-2829
43. M. Abdallah, A.M. El-Dafrawy, M. Sobhi, A.H.M. Elwahy, M.R. Shaaban. Inhibiting effects and theoretical studies of synthesized novel bisamino-thiazole derivatives as corrosion inhibitors for carbon steel in sulphuric acid Solutions. Int. J. Electrochem. Sci.,9 (2014) 2186-2206
44. O.A. Hazzazi, M. Abdallah, E.A.M. Gad. Inhibition effect of some cationic surfacants on corrosion of carbon steel in sulphuric acid solutions: surface and structural properties, Int. J. Electrochem Sci., 9(5), (2014) 2237-2253
45. J. Fu, Q. Zhou, Z. Liu, T. Liu. Effects of external stresses on hot behaviour of stainless steel TP347HFG. Corros. Sci.,104(2016) 103-111
46. B.A Pint. High-temperature corrosion in fossil fuel power generation: Present and future. Jorn. Mater.,65 (2013) 1024-1032
47. Y.G. Avdeev, Y.I. Kuznetsov, A.K. Buryak, Inhabitation of steel corrosion by unsaturated aldehydes in solution of mineral acids, Corros. Sci. 69 (2013) 50-60
48. K. Advdour, R. Touir, Y. Ramli, R.A. Belakhmima, M. Ebn Touhami, C. Mubengayi, H. El Kafsaoui, E.M. Essassi. Comparative inhabitation study of mild steel corrosion in hydrochloric acid by new class synthesized quinoxaline derivatives: Part 1, Res. Chem. In termed. 49 (2013) 1843-1855.
49. Q.B. Zhang, Y.X. Hau, Corrosion inhibition of mild steel by alkylimidazolium ionic liquids in HCl. Electrochimica. Acta. 54 (2009) 1881-1887

50. J. Savanya, P. Southari, K. Parameswari, S. Chitra.,Acenaphthol [1,2-b] pyrazine as corrosion inhibitors for mild steel in acid medium, Measurement. 77 (2016) 175-185
51. Z. Lei, C. Dai, B. Chen, Gas solubility in ionic liquids. Chem Rev. 144 (2014) 1289-1326
52. (a): H. Huang, Z. Dong, Z. Chen, X. Guo. The effects of ion concentration and relative humility on atmospheric corrosion behaviour of PCB-Cu under absorbed thin electrolyte layer. Corros. Sci. 53(2011) 123-1236; (b): M. R. Ezhilarasi, B. Prabha, T. Santhi, Novel Pyrazole Based Ionic Liquid as a Corrosion Inhibitor for Mild Steel in Acidic Media, Chem. Sci. Tran., 4 (2015) 758-767; (c): K. M. Manamela, L. C. Murulana, M. M. Kabanda, E. E. Ebenso, Adsorptive and DFT Studies of Some Imidazolium Based Ionic Liquids as Corrosion Inhibitors for Zinc in Acidic Medium, Int. J. Electrochem. Sci., 9 (2014) 3029 – 3046.
53. M. Shukla, S. Saha, Relationship between stabilization energy and thermo physical properties of different Imidazolium ionic liquids: DFT Studies. Comp. Theor. Chem., (2013) 27-33.
54. K.R. Seddon, A. Stark, A.J. Torres. Influence of chloride, water and organic solvents on the physical properties of ionic liquids. Pure Appl. Chem. 72 (12)(2012) 2275-2287
55. A.J. Abdul Nasser et al. Absorption and corrosion inhibition of mild steel in hydrochloric acid medium by N-[Morphdin-4yl (phenyl) methyl] Benzamide. Int. J. Eng. Science. 2 (11), (2010) 248-258
56. A.O. James, N.C. Oforka, Olesugun, K. Abiola. Inhibition of acid corrosion of mild steel by zyridoxal hydrochloride. Int. J. Electrochem. Sci. 2 (2007) 278-284
57. V.R. Saliyan, A.V. Adhikari. Corrosion inhibition of mild steel in acid media by Quinoliny/thiopropano hydrazine. Indian J. Chem. Tech. 16 (2)(2009) 162-174
58. M. Scendo, J. Uzuanska. Inhibition effect of-butyl-4-Methy/pyridinium tetra-fluoroborate on the corrosion of copper in phosphate solution. Inter. J. Corros., 2011 (2011) 1-12.
59. G. Gece, The use of Quantum chemical methods in corrosion inhibitor studies. Corros. Sci., 50 (2008) 2981-2992

60. A. Chakrabarti, Quantum chemical study of the corrosion inhibition of mild steel in 6 percent (wt/wt) HCl by means of cyanognanidine derivatives. Br. Corros. J., 19 (1984) 124-126
61. J.M. Costa, J.M. Lluch. The use of quantum mechanics calculations for the study of corrosion inhibitors. Corros. Sci., 11 (1984) 929-933
62. R. Sayos, M. Gonzales, J.M. Costa. On the use of quantum chemical methods as an additional tool in studying corrosion inhibitor substances. Corros. Sci.11 (1986) 927-934
63. G. Bereket, C. Ogretir, A. Yurt. Quantum chemical calculation of some 4-Methyl-5-Substituted imidazole derivatives as acidic corrosion inhibitor for zinc. J. Mol. Struct.,(THEOCHEM).571 (2001) 139-145
64. G. Bereket, E. Hur, C. Ogretir. Quantum chemical studies on some imidazole derivatives as corrosion inhibitors for iron in acid medium. J. Mol. Struct.(THEOCHEM).,578 (2002) 79-88
65. D. Rabison, Spilitting Multiple bonds: a comparison of Methodologies on the accuracy of bond dissociation energies. J. Comput. Chem. 34 (2013) 2625-2634
66. A. Lupan, R. Bruce-King. Comparison of hypo electronic deltahedral ditechnetaboranes having eight to twelve vertices with their rhenium analogues: examples of polyhechal surface Metal-Metal multiple bonds. Polyhedron., 60 (2013) 151-157.
67. E.A. Hoffmann, R. Rajko, U.Z.A. Fekete, T. Kortvelyesi. Quantum chemical characterization of Abraham solvation parameters for gas-liquid chromatographic stationary phase. J. Chromatography A., 1216 (48), (2009) 8525-8544.
68. G. Baranovic, Intramolecular resonance-assisted hydrogen bonds: A theoretical description by means of atomic charges and charge fluxes. Spectrochim.Acta part A: Mol. Bio. Spect., 117 (2014) 465-472.
69. D.T.I. Nakazato, E.L. De Sa, R.L.A. Haiduke, An atomic charge study of highly ionic diatomic Molecular Systems. Int. J. Quantum Chem., 110 (2010) 1729-1737.
70. R.S. Mulliken. Electronic population analysis on LCAO-MO molecular wave functions. J. Chem. Phys. 36 (1955)1833-1846.

71. R.S. Mulliken. Criteria for construction of good self-consistent-field molecular orbit wave functions and significance of LCAO-MO population analysis. J. Chem. Phys. 36 (1962) 3428-3439.

72. N.T. Yakhanthip, J. Kangwan, P. Jitonnom, S. Anuraqudom, J. Suttiwong, S. Hannongbua, Theoretical investigation on the electronic and optical properties of poly (flurenevinylene) derivatives as light-emitting materials. Int. J. Photoenergy., 2011 (2011) 9 – 18

73. Y.S. Mary, C.Y. Panicker, M. Sapuakumari, B. Narayan, B.K. Sarojini, A.A. Al-Saadi, C. Van Alsenoy, J.A. War, H.K. Fun. Molecular structure, FT-IR, Vibrational assignment Homo-Lumo analysis and molecular docking study of 1-[5-(4-Bromophenyl)-3-(4-fluorophenyl)-4,5-dihydro-1H-pyrazol-1-yl]ethanone. Spectrochim. Acta A:Mol. Biomol., 136 (2015) 473-482

74. A. Najiya, C.Y. Panicker, M. Sapuakumari, B. Narayan, B.K. Sarojini, C. Van Alsenoy. Molecular structure, FT-IR, first order hyperpolarizability, NBO analysis, HOMO-LUMO, MEP analysis of (E) -3-(4-chlorophenyl)-1-(4-fluorophenyl) prop-2-en-1-one by HF and density functional methods. Spectrochim. Acta A: Mol. Biomol. Spectrosc., 133 (2014) 526-533

75. B.W. D'Andrade, S. Datta, S.R. Forrest, P. Djurovic, E. Polikapov, M.E. Thompson. Relationship between the ionization and oxidation potentials of molecular organic semiconductors. Org. Electron., 6 (2005) 11-20

76. P.G.H. Saudar. enhancement factor for the electric dipole moment of the valence electron in an alkali atom. Phys. Letters., 22 (1966) 290-291

77. R.P. Iczkowski, J.L. Margrave. Electronegativity. J. Am. Chem. Soc., 83 (17)(1961) 3547-3551

78. D.W. Smith. A new approach to the relationship between bond energy and electronegativity. Polyhedron., 26 (2007) 519-523.

79. S. Kaya, C. Kaya. A new equation based on ionization energies and electron affinities of atoms for calculating of group electronegativity. Comput. Theoret. Chem., 1052 (2015) 42-46.

80. N. Islam. Correlation between the electronegativity ansatz of Mulliken and Gordy. J. Mol. Struct.(THEOCHEM)., 947 (2010) 123.

81. J.E. Huheey. The electronegativity of groups. J. Phys. Chem., 69 (1965)3284-3291.

82. R.G. Pearson. Electronegativity scales Acc. Chem. Res., 23 (1990) 1-2

83. P.W, Ayers, R.G. Parr. Beyond electronegativity and local hardness: higher-order equalization criteria for determination of a group-state electron density. J. Phys. Chem. A., 115 (2011)8528-8531.

84. S.S. Batsanov. The concept of electronegativity conclusions and prospects. Rus. Chem. Rev., 37 (1968) 332-351.

85. R. Hasanov, M. Sadikoglu, S. Bilgic, Electrochemical and quantum chemical studies of some Schiff bases on corrosion of steel in H_2SO_4 solution. Appl. Surf. Sci., 253 (2007) 2913-2921.

86. J.M. Roque, T. Pandiyan, J. Cruz, E. Garcla-Ochoa. DTF and electrochemical studies of tris (benzimidazole-2-ylmethyl) amine as an efficient corrosion inhibitor for the carbon steel surface. Corros. Sci., 50 (2008) 614-624.

87. R.G. Pearson. Absolute electronegativity and hardness concluded with molecular orbital theory. Proc. Natl. acad. Sci. USA., 83 (1986) 8440-8441.

88. F. Kandemirli, S. Sagdinc. Theoretical study of corrosion inhibition of amides and Thiosemicarbazones. Corros. Sci., 49 (2007) 2118-2130.

89. T. Mineva. Selective study from the density functional local reactivity indices. J. Mol. Stuct: THEOCHEM., 762 (1-3),(2006) 79-86.

90. R.G. Parr, W. Yang. Density functional Theory of atoms and molecules. Oxford University Press, New York 1 (1986), 1-39.

91. M. Berkowitz. Density functional approach to frontier controlled reaction. J. Am. Chem. Soc., 109 (1987) 4823-4825.

92. B. Zerga, B. Hammouti, M. Bennajeh, M. Ebn-touhami, R. Touir, M. Taleb, M. Sfaira, I. Forsaal, Comparative inhibition study of new synthesized pyridazine derivatives towards mild steel corrosion in hydrochloric acid. Part II Thermodynamics properties. Int. J. electrochem. Sci., 7 (2012) 471-483

93. I. Lukovits, E. Kalman, G. Palinkas, Non – Linear group – contribution models of corrosion inhibitors, Corros., 51 (3), (1995) 201- 205.

94. T. Rajamani, S. Muthu, Vibration spectra, first order hyperpolarizability, NBO, fukui function and HOMO-LUMO analysis of 2-[4-(1.3-benzodioxol-5-ylmethyl)-

1-pipezinyl] pyrimidine. Spectrochimia Acta part A: Mol. Bio. Spect., 115 (2013) 654-667.

95. G.R. Ramkumaar, S. Srinivasan, T.J. Bhoopathy, Molecular geometry, vibrational spectra atomic charges, frontier molecular orbital and Fukui function analysis of drug zidovadine, Spectrochim Acta part A: Mol. Bio. Spect., 99 (2012) 189-195.
96. L. Larabi, O. Benali, S.M. Mekelleche, Y. Harek, 2-mercapto-1-methylimidazole as corrosion inhibitor for copper in hydrochloric acid. App. Surf. Sci., 253 (3)(2006) 1371-1378.
97. J.U. Maheswari, S. Muthu, T. Sundius. QM/MM methodology, docking and spectroscopic (FT-IR/FT-Raman, NMR, UV) and Fukui function analysis on adrenergic against. Spectrochim. Acta part A: Mol. Bio. Spect., 137 (2015) 841-855.
98. A.B. Tadros, A.B. Adbennabey, Inhibition of the acid corrosion of steel by 4-amino-3-hydrazino-5-thio-1, 2, 4-triazoles 5. Electroanal. Chem., 24 (1988) 433-439.
99. S.S. El-Rehim, M.A.M. Ibrahim, K.F. Khaled, 4-Aminoantipyrine as an inhibitor of mild steel corrosion in HCl solution. J. Appl. Electrochem., 29 (1999) 593-599.
100. M. Bouklah, B. Hammouti, M. Lagrenee, F. Bentiss, Thermodynamics properties of 2,5-bis(4-methoxyphenyl)- 1,3,4-oxidiazole as a corrosion inhibitor for mild steel on normal sulphuric acid medium. Corros. Sci., 48 (2006) 2831-2842.
101. M. Elayyachy, M. Elkodadi, A. Aouniti, A. Ramdani, B. Hammouti, F. Malek, A. Eldvissi, New bipyrazole as corrosion inhibitors for steel in hydrochloric acid solutions. Mater. Chem. Phys., 93 (2005) 281-285.
102. C. Fraqoza-Mar, O. Olivares-Xometl. M.A. Douringuez- Aquilar, E.A. Flores, P. Arellanes-Lozada, F. Jimenez Cruz. Corrosion inhibitor activity of 1,3-diketone malonates for mild steel in aqueous hydrochloric acid solution. Corros. Sci. 61 (2012) 171-184.
103. Y.G. Avdeev, Y.I. Kuzvetsov, A.K. Buryak, Inhibition of steel corrosion by unsaturated aldehydes in solutions of mineral acids. Corros. Sci., 69 (2013) 50-60.

104. L. Herrag, B. Hammouti, A. Aouniti, S. El Kadiri, R. Touzani, Effect of diaminoalkane derivatives on mild steel corrosion in HCl media, Acta. Chim. Slov., 54(2007) 419-423.

105. I.B. Obot, N. Obi-Egdebi, S.A. Umoren, E.E. Ebenso. Absorption and kinetic studies on the inhibition potential of fluconazole for the corrosion of Al in HCl solution. Chem. Eng. Commun., 198 (2011) 711-725.

106. Z. Xu, N.J. Singh, S.K. Kim, D.R. Spring, K.S. Kim, J. Yoon. Induction-Driven Stabilization of the Anion- π interaction in electron rich aromatics as the key to fluoride conclusion in Imidazolium Cage Receptors. Eur. J., 17 (4)(2011) 1169-1170.

107. H. Ashassi-Sorkhabi, D. Seifzadeh, M.G.E.N. Hossein, EIS and polarization studies to evaluate the inhibition effect of 3H-phenothiazin-3-one,7-dimethylamin on mild steel corrosion in 1M HCl solution. Corros. Sci., 50 (2008) 3363-3370.

108. A. Popova, M. Christova, Evaluation of impedance measurements on mild steel corrosion in acid media in the presence of heterocyclic compounds. Corros. Sci., 48 (2006) 3208-3221.

109. D.A. Lopez, S.N. Simison, S.R. DeSanchez, The influence of steel micro structure on CO_2 corrosion. EIS on the inhibition efficiency of benzimdazole. Electrochim. Acta., 48 (2003) 845-854.

110. K.F. Khaled. The inhibition of benzimidazole derivatives of iron in 1M HCl solution. Electrochim. Acta. 48 (2003) 2493-2503.

111. A.K. Singh, M.A. Quraishi, The effects of some bis-thiazole derivatives on the corrosion of mild steel on hydrochloric acid. Corros. Sci. 52 (2010) 1373-1385.

112. T.C. Girija, M.V. Sangaranarayanan, Analysis based of polyanilino-based nickel electrodes for electrochemical supercapacitors. J. Power Sources, 156 (2006) 705-711.

113. S. Vishwanatham, A. Kumar, Corrosion inhibition of mild steel in binary acid mixtures, Corros. Rev., 23 (2005) 181-194.

114. U. Retter, A. Widmann, K. Siegler, H. Kahlert. On the impedance of potassium nickel (ii) hexacyanoferrate (ii) composite electrodes- the generalization of the randles model referring to inhomogeneous electrode. J. Electroanal Chem. 546 (2003) 87-96.

115. L.O. Olasuukanmi, I.B. Obot, M.M. Kabanda, E.E. Ebenso, Some Quinoxalin-6-yl derivatives as corrosion inhibitors for mild steel in hydrochloric acid: Experimental and theoretical studies. J. phys. Chem., 199 (2015)16004-16019.

116. S. H. Kumar, S. Kathikeyan, Torsemide and furosemide as green inhibitors for the corrosion of mild steel in hydrochloric acid medium. Ind. Eng. Chem. Res., 52 (2013)7457-7469.

117. D.K. Yadav, M.A. Quraishi. Electrochemical investigation of substituted pyrano pyrazoles absorption on mild steel in acid solution. Ind. Eng. Chem. Res. 51 (2012) 8194-8210.

118. Y. Jeon, J. Sung, C. Seo, H. Lim, H. Cheong, M. Kang. B. Moon, Y. Ouchi, D. Kim. Structure of ionic liquids with different anions studied by infrared vibration spectroscopy. J. Phys. Chem. B. 112 (2008) 4735-4740.

119. D. Forster, D.M.L. Goodgame. Infrared spectra (400-200cm^{-1}) of thiocyanate and isothiocyanate complexes. Inorg. Chem. 4 (1965) 715-718.

120. M. Yadav, S. Kumar, I. Bahadur, D. Ramjugernath, Corrosion inhibitive effect of synthesized thiourea derivatives on mild steel in a 15 % HCl solution. Int. J. Electrochem. Sci. 9 (2014) 6529-6550.

121. S. Yeganegi, V. Sokhanvaran, A. Soltanabadi, Study of thermodynamic properties of imidazolium-based ionic liquids and investigation of true alkyl chain length effect by molecular dynamic simulation. Molec. Simul., 39 (2013)1070-1078.

122. Y.X. Fan, K.Q. Lai, B.A. Rasco, Y.Q. Huang. Analysis of phosmet residues in apples with surface - enhanced Raman spectroscopy. Food Control. 37 (2014) 389-395.

123. H. Fang, X. Zhang, S.J. Zhang, L. Liu, Y.M. Zhao, H.J. Xu, Ultra-sensitive and quantitative detection of paraquat on fruits via surface-enhanced Raman spectroscopy. Sens. Actuators B. Chem., 213 (2015) 452-456.

124. B. Gomez, N.V. Likhanova, M.A. Dominguez-Aguilar, R. Martinez-Palou, A. Vela, J.L. Gazquez, Quantum chemical study of the inhibitive properties of 2-pyridyl-Azoles. J. Phys. Chem. B., 110 (2006) 8928-8934.

125. C.B.P. Kumar, K.N. Mohana, H.B. Muralidhara, Electrochemical and thermodynamic studies to evaluate the inhibition effect of synthesized piperidine

derivatives on the corrosion of mild steel in acidic medium. Ionics., 21 (2015) 263-281.

126. F. Karadag, I. Dehri, M. Ozcan, L. Murulana, I.B. Obot, M.M. Kabanda, E.E. Ebenso, Quantum chemical studies on the corrosion of mild steel by some triazoles and benzimidazole derivatives in acidic medium. Int. J. Electrochem. Sci., 7 (2012) 5035-5056.
127. K.F. Khaled B. Hammouti , A.K. Singh, M.A. Quraishi, L. Murulana, I.B. Obot, M.M. Kabanda, E.E. Ebenso, N. Eddy. Quantum chemical investigations on quinolone derivatives as effective corrosion inhibitors for mild steel in acidic medium. Int. J. Electrochem. Sci., 7 (2012) 5643-5676.
128. I.B. Obot, M.M. Kabanda, E.E. Ebenso, Computational study of some amino acid derivatives as potential corrosion inhibitors for different metal surfaces and in different media. Int. J. Electrochem. Sci., 8 (2013) 10839-10850.
129. N.O. Eddy, E.E. Ebenso, I.U. Ibok, A. El Nemr, H.E. El Ashry, Quantum chemical study of the inhibition of the corrosion of mild steel in H_2SO_4 by some antibiotics. J. Mol. Model., 15 (2009) 1085-1096.
130. F.E. Awe, C.E. Gimba, N.O. Ibisi, E.E. Ebenso, N. Eddy QSAR, Experimental and computation chemistry. Simulation studies on the inhibition potentials of some amino acids for the corrosion of mild steel in 0.1M HCl. Int. J. Electrochem. Sci,. 6 (2011) 6931-6957.

APPENDIX: FORMULAS USED

---

1. **Electronegativity:**

$$\chi \cong -\tfrac{1}{2}\,(E_{HOMO} + E_{LUMO})$$

2. **Global hardness:**

$$\eta \cong -\tfrac{1}{2}\,(E_{HOMO} - E_{LUMO})$$

3. **Energy Gap**

$$\Delta E = E_{LUMO} - E_{HOMO}$$

4. **Global softness:**

$$\sigma = 1/\eta \cong -2/(E_{HOMO} - E_{LUMO})$$

5. **Electron affinity related to E_{HOMO} :**

$$I \cong - E_{HOMO}$$

6. **Electron affinity related to E_{LUMO} :**

$$A \cong - E_{LUMO}$$

7. **Potentiodynamic polarization inhibition efficiency:**

$$\mu_{PDP} = \frac{i^{0}_{corr} - i^{i}_{corr}}{i^{0}_{corr}} \times 100$$

8. **Electrochemical impedance spectroscopy inhibition efficiency:**

$$E_{EIS}\,\% = \left(1 - \frac{R^{0}{}_{ct}}{R_{ct}}\right) \times 100$$

9. **Surface coverage (with thermodynamic parameters):**

$$\theta = \frac{K_{ads} C_{inh}}{1 + K_{ads} C_{inh}}$$

10. **Surface coverage (with thermodynamic parameters) rearranged:**

$$\frac{C_{inh}}{\theta} = \frac{1}{K_{ads}} + C_{inh}$$

11. Surface coverage (with thermodynamic parameters) for Temkin

$$\theta = -\frac{1}{2_a}(\ln K_{ads} + \ln C)$$

12. Current response, constant phase element:

$$Z_{CPE} = Y_0^{-1}(i\omega)^{-n}$$

13. Double layer capacitance:

$$C_{dl} = (Y_0 R_{ct}^{1-n})^{1/n}$$

14. Thickness of the protective layer (d):

$$C_{dl} = \frac{\varepsilon\varepsilon_0}{d}$$

15. Surface coverage (EIS):

$$\theta = 1 - \frac{R^0_{ct}}{R_{ct}}$$

16. Nucleophilic Fukui function:

$$f^+ = q_{(N+1)} - q_N$$

17. Electrophilic Fukui function:

$$f^- = q_N - q_{(N-1)}$$

18. Gibbs free energy of adsorption:

$$k = \frac{1}{55.5}\exp\left[\frac{-\Delta G^o_{ads}}{RT}\right]$$